UNIVERSITÀ DEGLI STUDI DI PADOVA

Scuola di Scienze

Dipartimento di Geoscienze

Direttore: Prof. Fabrizio Nestola

Corso di Laurea in Geologia e Geologia Tecnica

Characterization of metallurgical slags towards the formulation of alternative binders

Relatore: Prof. Gilberto Artioli

Correlatori: Dott. Maurizio Bellotto

Dott.ssa Maria Chiara Dalconi

Laureanda: Veronica Pasinato

Matricola 1147160

Anno Accademico 2017/2018

Contents

Abstract III
Riassunto V
1. Introduction 1
2. Overview 3
2.1 Present situation and Circular Economy 3
2.2 About Portland Cement 10
2.2.1 Portland cement production 10
2.2.2 Hydration process 11
2.2.3 Cements classification 13
2.3 EAF (Electric Arc Furnace) and BOF (Basic Oxygen Furnace) production 15
2.4 Foundry process 18
2.5 About steel slags 19
2.5.1 Mineralogical properties of BOFs and EAFs 21
3. Characterization and materials 23
3.1 X-ray fluorescence (XRF) 24
3.1.1 Sample preparation 24
3.2 X-ray powder diffraction (XRD) 25
3.2.1 Sample preparation 25
3.2.2 Quantitative analysis of hydration products 28
3.3 Scanning Electron Microscope (SEM) 28
3.3.1 Sample preparation 29
3.4 Laser granulometry 30
3.5 Calorimetry 31
3.6 Mechanical Strength 31
3.6.1 Sample preparation 32
3.6.2 Splitting and compression tests 33
3.6.3 Experimental Design 37
4. Results and discussion 39
4.1 X-ray fluorescence (XRF) 39
4.2 X-ray powder diffraction (XRD) 42
4.2.1 XRD of hydration products 47
4.3 Scanning Electron Microscope (SEM) 49

4.3.2 BSE Images and EDS Spectra 49
4.4 Calorimetry 52
4.5 Laser granulometry 59
4.6 Mechanical Strength 60
5. Conclusions 69
Appendix A - Hydration phases XRD diffractograms 71
Appendix B - BSE Images and EDS Spectra (SEM) 77
References 87
Acknowledgements/Ringraziamenti 89

Abstract

The large CO_2 emissions which come from limestone calcination, one of the raw materials to produce Portland cement, pose an urgent global issue that requires industrially sustainable alternative options to replace this material.

This work is about the characterization of three types of metallurgical slags from Italian companies, two of them are from steel mills (with an EAF production process) and the other one from foundry process. We try to find if we can take advantage of these waste materials as supplementary cementitious materials, encouraging the use of local products to produce eco-sustainable binders.

The analyses done give us information about the elementary chemical composition, by the X-ray fluorescence, the mineralogic composition, by X-ray powder diffraction, and the particle size distribution by laser granulometry. Calorimetric data are important to assess the behaviour and the reactivity of the different slags in the cementitious formulations. Mechanical compressive and splitting test determine the mechanical strength of the formulations.

The two slags from steel mills are reactive, show quick setting (due to their abundance in mayenite), and thus they need the addition of GBBS and gypsum to slow down their reactivity.

The slag from the foundry process is not much reactive, it does not have problems of quick setting and expansive reactions and it can be mixed to the cement as it is, without the addition of GBBS.

By choosing the correct quantity of slag, GBBS and gypsum mixed together in different formulations, these materials can reach mechanical strength classes of 32.5 MPa and 42.5 MPa.

Riassunto

Le enormi emissioni di CO_2 che provengono dalla calcinazione del calcare, uno dei materiali grezzi per produrre il cemento Portland, pongono un urgente problema a livello globale che richiede opzioni alternative industriali sostenibili per sostituire questo materiale.

Questo lavoro riguarda la caratterizzazione di tre tipi di scorie metallurgiche provenienti da stabilimenti italiani. Due di queste provengono da acciaierie che utilizzano un processo di fusione di arco elettrico, l'altra viene da una fonderia. Abbiamo cercato di capire se riuscivamo a sfruttare questi materiali di scarto per usarli come materiali cementizi aggiuntivi, incoraggiando l'uso di prodotti locali per produrre leganti alternativi.

Le analisi fatte ci danno diverse informazioni riguardo alla composizione chimica elementare delle scorie, determinata con la fluorescenza a raggi X, la composizione mineralogica, con la diffrazione a raggi X da polveri, e la granulometria (con un granulometro laser). I dati calorimetrici sono importanti per stimare il comportamento e la reattività delle scorie. I test meccanici di compressione e trazione determinano la resistenza meccanica delle formulazioni.

Le due scorie di acciaieria sono reattive e mostrano presa rapida (dovuta alla presenza di mayenite), quindi hanno bisogno dell'aggiunta di loppa e gesso per rallentare la presa.

La scoria di fonderia non è molto reattiva, non ha problemi di presa rapida o reazioni di espansione e può essere mischiata al cemento così com'è, senza l'aggiunta di loppa.

Scegliendo la giusta quantità di scoria, loppa e gesso, mischiati insieme in diverse formulazioni, questi materiali possono raggiungere resistenze meccaniche di 32.5 MPa e 42.5 MPa.

Chapter 1

Introduction

Portland cement is the most used material on global scale, right after water, and its total production is estimated around 2.6 billion tonnes in 2008. Global anthropogenic CO_2 emissions from cement production amount to 5-8% of the total. (Van Deventer *et al.*, 2012, data of 2008).

The production of cement is an energy-intensive process and requires approximately 4.000 MJ/t of cement, which includes the grinding of raw materials, their calcination at 1500°C and the grinding of raw materials (Shi, 2004).

The success of this material lays in its good mechanical properties, durability, in the low cost and wide availability of the raw materials used (clay, limestone and gypsum) and in its by now optimized production process. The principal problem is the production of CO_2 as by-product.

Facing problems like global climate changes and high amount of CO_2 emissions, which largely comes from the decomposition of limestone during Ordinary Portland Cement (OPC) production, it's time to look out for alternative options, possibly using recycled materials, in order to obtain sustainable solutions for the future.

With the substitution of Portland cement clinker by GBBS in cement and concrete, the consumption of natural raw materials as well as energy demands of cement production and specifically CO2 emissions are significantly decreased (Euroslag, 2018).

Besides the problem of the large CO_2 emissions, it is important to take advantage of industrial waste products like blast furnace slag and steel slags, encouraging the use of local products to produce eco-sustainable binders.

Steel slags are one of the largest fractions of by-products from the conversion of iron to steel in basic oxygen furnaces (BOF) or the melting of scrap to make steel in an electric arc furnace (EAF).

This kind of slags has cementitious properties and they are being used as an asphalt concrete aggregate in most countries.

The use of steel slags as cementitious addition is not a frequent case, but this is the aim of this work: to use it as a replacement for cement towards different formulations with alternative binders.

Chapter 2

Overview

2.1 Present situation and Circular Economy

Under the 2009 Copenhagen Agreement[1], more than 120 countries have agreed to keep the global average temperature increase below 2°C. This maximum acceptable temperature increase is based on recommendations from numerous scientific studies, warning that increases larger than 2°C can trigger dangerous anthropogenic interference with the climate system, with serious consequences to water supply, agricultural productivity, sea-level rise, human habitability and global security (Van Deventer *et al.*, 2012).

Precisely in this agreement, it has been underlined that climate change is one of the greatest challenges of our time and many scientists estimate that the concentration of CO_2 has already exceed the safe level *(Figure 2.1),*(Ramanathan and Xu, 2010). Obviously, it's a delicate argument to discuss about and not everyone agrees that this is a serious problem to face, especially the mining industries, but there is economic and social benefit in reducing CO_2 emissions and valorising waste materials at the same time.

[1] *The Copenhagen Agreement* is a document that delegates at the 15th session of the Conference of Parties (COP 15) to the United Nations Framework Convention on Climate Change agreed to "take note of" at the final plenary on 18 December 2009.

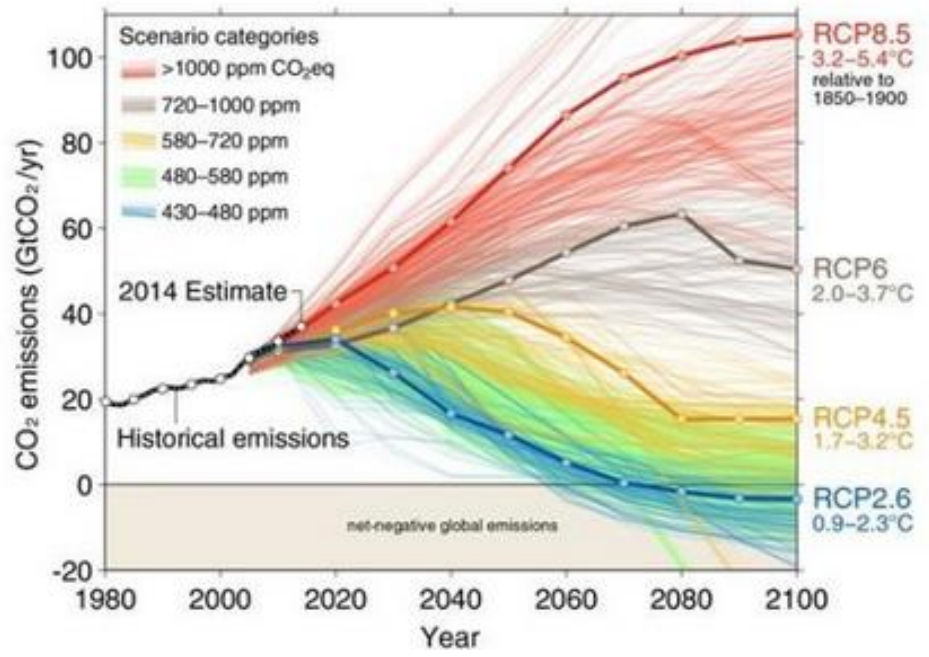

Figure 2.1. Future scenarios of CO_2 emissions from 1980 to 2100. These are at least 1200 scenarios of future emissions, based on peak concentration of CO_2 emissions: each of it has a different "story" of how the future might be. (CICERO-Centre for International Climate and Environmental Research, 2014).

Concrete made from Ordinary Portland Cement (OPC), including its blends with mineral admixtures, is second only to water as the commodity most used by mankind today *(Figure 2.2)*. Global cement production in 2008 was around 2.6 billion tonnes, contributing conservatively 5-8% of global anthropogenic CO_2 emissions (Van Deventer *et al.*, 2012).

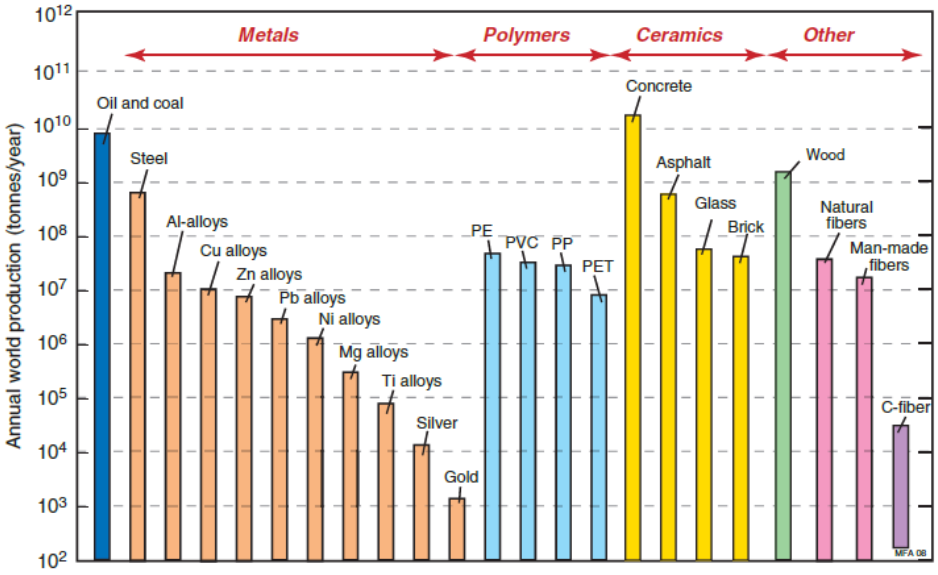

Figure 2.2. The annual production (in a logarithmic scale) of the most used materials in the current days, on which the industrialized society depends. (Ashby, 2009). We can see from the figure how high is the production of concrete in absolute values and also compared to the other materials.

About energy, it is known that there are different ways to obtain it from various sources, all of them are finite, but for the energy that comes from the sun and from tidal waves the time scale for the exhaustion is so large that it is safe to regard them as infinite (Ashby, 2009). It is not the same thing for hydrocarbon fuels, but as it can be seen from *Figure 2.3*, the world annual consumption is extremely high.

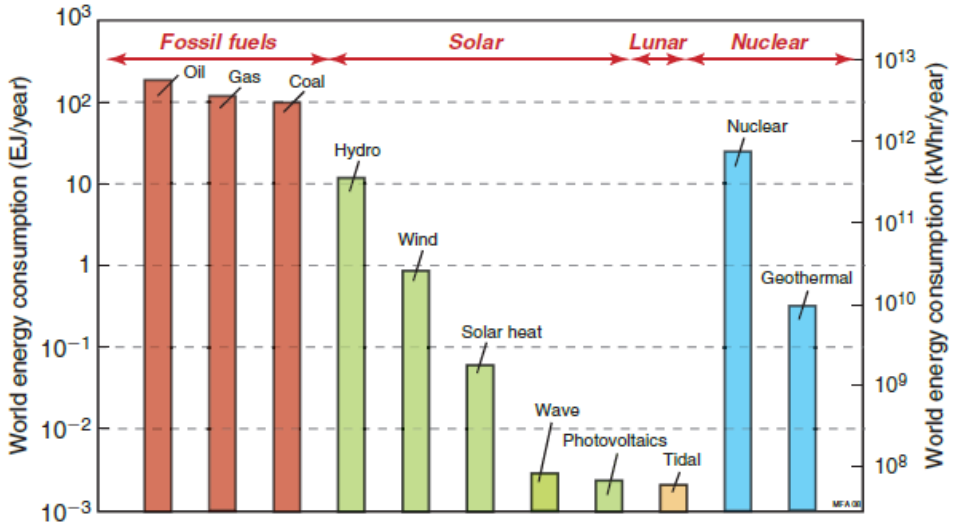

Figure 2.3. The annual energy consumption in the whole world (logarithmic scale). Data from 2005 (Nielsen, 2005). (Ashby, 2009).

The industry uses materials that are drawn from Earth's reserves of minerals[2], but these resources[3] have limits. With the growth of the world's population the demand for energy and materials is also increasing. The growth of demand is exponential and for most materials it accounts for between 3% and 6% per year (Ashby, 2009). This large growth obviously has consequences on our planet. Mineral resources are not infinite and the balance between demand and supply can be disrupted. This could cause scarcity of the source and increase prices.

[2] Mineral reserve: the part of a mineral which can be legally and economically extracted at a determinate time.
[3] Mineral resource: it is different from "reserve". It is the real total, it includes the current reserve and all usable deposits that might be available in the future.

About sustainability, *"Sustainable development is development that meets the needs of the present without compromising the ability of future generations to meet their own needs".*

This is the definition of "sustainable development" from the *Brundtland Report* of the World Council on Economic Development (WCED[4], 1987), which constitutes the basis of agreement for most people about what sustainability is (Ashby, 2009).

"Circular economy" (CE) is a good and reasonable way to start, it is a regenerative system with the purpose to reduce waste, emissions and energy leakage in order to recycle, reuse and refurbish. This "ideal closed loop" is not respected and we are now reaching limits in the way we use our sources, from fossils fuels to the energy required to produce new materials.

The CE has not a single global definition, many different recent definitions can be found, from international organisations, non-governmental organisations and academia. For example, in Europe, CE has been defined as *"a way to keep the added value in products for as long as possible and eliminate waste"* (de Jesus *et al.*, 2018) and a way to *"boost the EU's competitiveness by protecting businesses against scarcity of resources and volatile prices, helping to create new business opportunities and innovative, more efficient ways of producing and consuming"* (de Jesus *et al.*, 2018).

Another definition is: *"Central elements of the circular economy include remanufacturing and product life-cycle extension schemes such as re-use and refurbishment"* (de Jesus *et al.*, 2018).

Anyway, all the different definitions contain the principal elements of which the CE is about:

- Input minimisation and efficient use of regenerative resources, with a particular attention on the renewable energy
- Life cycle extension and systems reconceptualization (re-using and recycling)
- Output reduction valorisation and waste minimization

[4] WCED: World Commission on Environment and Development.

In cement manufacturing CO_2 emissions are due mainly to the decomposition of limestone (OPC's raw material), the combustion of fossil fuels during cement production and the transport of these products.

The cement industry has started look for alternative strategies to reduce the impact of cement *(Figure 2.4)*, using alternative binders in a carbon constrained industry, given that there are significant reductions in CO_2 emissions.

Facing this problem, there is a significant potential to reduce the demand for new cement, using other materials (in *Figure 2.5* their chemical composition can be seen), such as blast furnace slags, steel slags, alkali-activated binders, fly ashes and marble powder, which are produced with less emissions than ordinary Portland cement.

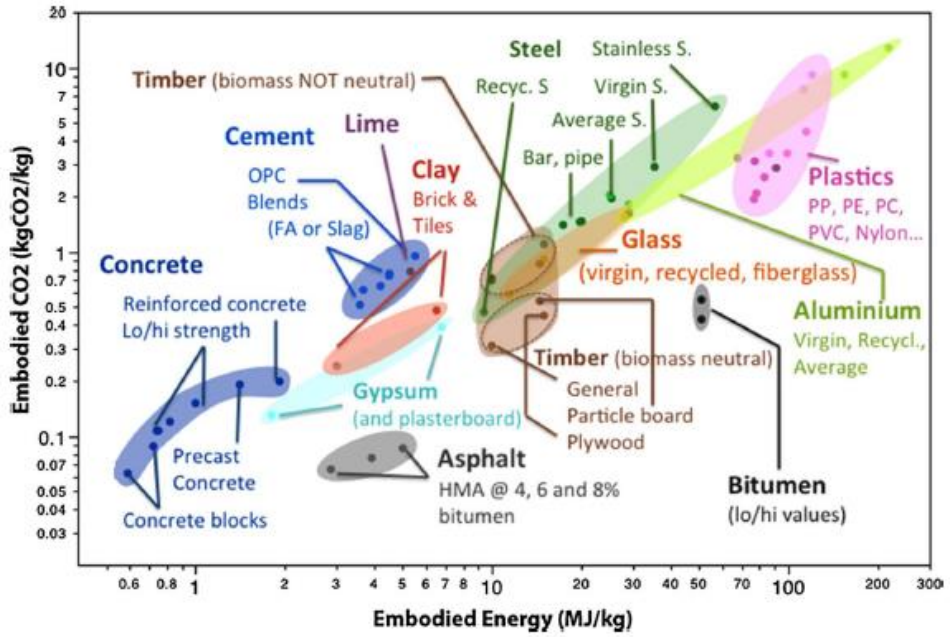

Figure 2.4. Embodied CO_2 and energy for materials typically used in the construction industry (Barcelo et al., 2008). It shows that concrete has a low fingerprint for unit weight, but it is used in such huge volumes that globally it has a high impact, differently, cement's value is higher because it has no aggregates. All these materials follow a straight line in this graphic, except for the cement: it slightly distances itself due to the higher CO_2 emitted caused by the calcination of the limestone.

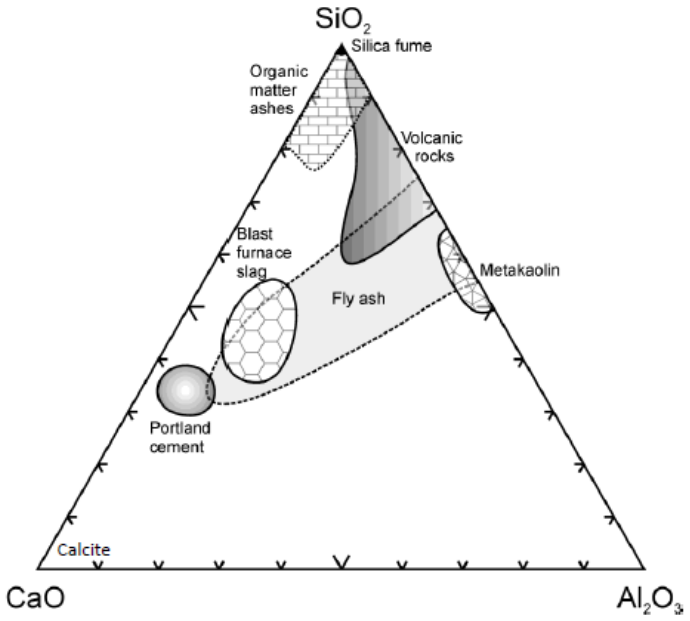

Figure 2.5. Ternary diagram of the chemical composition of some of the secondary cementitious materials (Snellings, Mertens and Elsen, 2012).

2.2 About Portland Cement

Portland cement is the most produced and used hydraulic binder, invented in 1824 in England by the bricklayer Joseph Aspdin, who named it “Portland cement” because it had a similar colour as the “Portland stone”, extracted in Dorset (England).

2.2.1 Portland cement production

This type of product is made of clinker (the firing product of clay and limestone), to which a small quantity of gypsum is added to control the aluminate reactions. Aluminates are necessarily present in clinker because at high temperature they constitute the liquid phase needed to speed up and lower the temperature of the clinkerisation reactions.

The production process can be divided in four phases:

1. Extraction, grinding, drying and homogenisation of the raw materials
2. Pre-calcination of the obtained flour
3. Clinkerisation process (1450°C)
4. Cooling process, grinding of the clinker grains and addition of sulphates and other mineral additions

The most abundant phases are four: Alite, Belite, Aluminate, Ferrite (*Table 2.1*).

The fineness of the product is very important because it influences the velocity of the reaction with water.
In addition to the major phases, there are some minor phases like periclase (MgO), free lime (CaO), Portlandite ($Ca(OH)_2$), but their presence is controlled (by the flame temperature accurately regulated) in order to be low (0-3%).

Phase	Chemical atom formula	Chemical oxide formula	Cement notation
Belite	Ca_2SiO_4	$2CaO \cdot SiO_2$	C_2S
Alite	Ca_3SiO_5	$3CaO \cdot SiO_2$	C_3S
Aluminate	$Ca_3Al_2O_6$	$3CaO \cdot Al_2O_3$	C_3A
Ferrite	Ca_2AlFeO_5	$4CaO \cdot Al_2O_3 \cdot Fe_2O_3$	C_4AF

Table 2.1. The four phases of clinker with their chemical atom and oxide formulas and cement notation.

2.2.2 Hydration process

The reactive Portland cement powder is mixed with water to produce a final hardened material through many complex reactions: the hydration process.

Hydration involves basically three processes: dissolution, supersaturation and precipitation. What happens is dissolution of the crystal phases, surface reactions, gel formation (caused by the small dimensions of the precipitates and the surface interaction between the particles) and new phases precipitation.

Obviously, the different crystal phases have different reactivities: C_3A is the most reactive and C_2S is the lowest. The reactivity of each phase depends on the presence of all the phases and on the composition of the interstitial solution.

The hydrated phases formed by the reaction of Portland cement and water are poorly-crystalline solids of variable composition: among them *C-S-H (Calcium Silicate Hydrate)*, where the main components are CaO, SiO_2 and H_2O *(Figure 2.6)*.

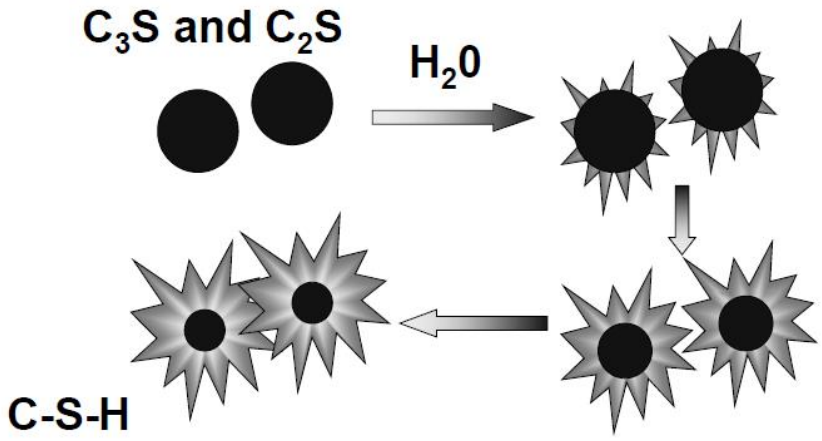

Figure 2.6. A schematic figure of the hydration process of C2S and C3S and the formation of C-S-H (Mazzoli, 2017).

The hydration of C_3A (mostly) and C_4AF *(Figure 2.7)* is very fast and it requires the addition of gypsum to slow down the fast-setting through the formation of ettringite.

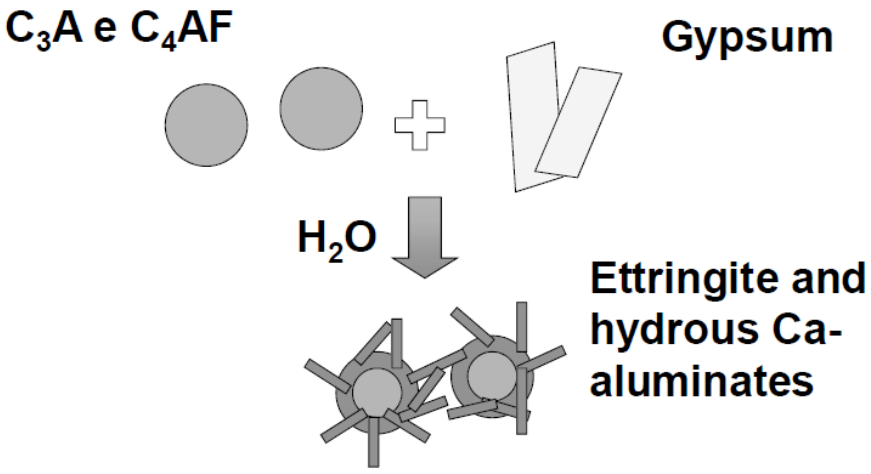

Figure 2.7. A schematic figure of the hydration process of aluminate phases and the formation of hydration products (Mazzoli, 2017).

This process leads to the formation of hydration products like ettringite (($Ca_6 Al_2(SO_4)_3 (OH)_{12} \cdot 26(H_2O)$), also called Aft, and monosulphate (AFm). Some of these products can create problems of expansivity if they form after setting, when cement paste has lost its plasticity (secondary formation): secondary ettringite (from Afm), thaumasite (from CH), especially in dump and polluted environments.

The completion of the hydration process may take days, months, or even years depending on the crystal size, the defectivity and polymorphism of the phases, the porosity of the paste and the environmental conditions.

Strength development is related to the degree of hydration and to the speed of the process: the faster the hydration kinetics, the faster is the strength development (Artioli, 2018).

2.2.3 Cements classification

At present many different types of cement exist: the norm used for the classification is the *UNI –EN 197-1, 2007*. This norm classifies the cements which can be used for structural purposes and it defines the compositional requirements and the compliance of cements (Dalconi, 2017).

According to the norm, which considers 5 types of cements, a cement must be identified by two characteristics: type of cement and strength class.

The five classes based on the first requirement are:

1. CEM I Ordinary Portland Cement
2. CEM II Composite Portland Cement
3. CEM III Blast Furnace Cement
4. CEM IV Pozzolanic Cement
5. CEM V Composite Cement

Except for Ordinary Portland Cement, each class has one or more subgroups, for a total of 27 different types of cements. Each subgroup can be supplied by the producer in one of the six strength classes: the normalized strength of a cement is determined by the *EN 197-1* with a compressive strength test done at 2, 7 and 28 days.

This norm dictates 3 strength classes:

1. 32.5 class
2. 42.5 class
3. 52.5 class

For each normalized strength class, the norm defines two initial strength classes:

1. N: ordinary strength class
2. R: class of rapid strength development

2.3 EAF (Electric Arc Furnace) and BOF (Basic Oxygen Furnace) production

Depending on the iron and steel production process different slag types are produced. The production of steel slags is due to the conversion of hot pig iron metal to crude steel in a Basic Oxygen Furnace (BOF) or during the melting of scrap in an Electric Arc Furnace (EAF).

If the crude steel undergoes further secondary steelmaking processes, different kinds of secondary metallurgical slags are formed.

BOF slags are formed during the conversion of hot metal from the blast furnace into steel in a basic oxygen furnace. In this kind of process, the hot metal is treated by blowing oxygen to remove carbon and other elements that have a high affinity to oxygen (Euroslag, 2018).

When the process is completed, the crude steel and the slag are tapped into separated ladles, then the slag (still liquid), is poured and cooled in order to form crystalline slags. Depending on the specific use, the crystalline slags undergo different processes like crushing or sieving.

This kind of slags has high surface hardness and it is an ideal aggregate for road constructions or surface layers for high abrasion resistance *(Figure 2.8).*

Figure 2.8. An example of Basic Oxigen Furnace slags (BOF), coarse aggregate (Euroslag, 2018).

EAF slags are different from the BOFs, this kind of slags is produced during the manufacture of crude steel by the electric furnace process, where electric current heats up the steel scrap (plus fluxes added) to a liquid state. Due to the different density, the slag floats on top of the molten steel and then it is tapped at high temperature (around 1600°C) and successively slowly cooled, forming crystalline slag (Euroslag, 2018).

After cooling the product from high temperatures (1580°C), the EAFs products become heavy, hard and a little bit porous and the initial colour is almost black, then it changes into light grey, due to the long-term outdoor weathering.

There are two types of EAFs, depending on the quality of the steel produced:

- EAF C: from carbon steel production
- EAF S: from stainless steel production

The EAFs are dense aggregates with a good resistance to deformation, they are ideal to use as aggregates for asphalt surface materials and road surface treatments *(Figure 2.9).*

Figure 2.9. An example of Electric Arc Furnace slags (EAF), coarse aggregate (Euroslag, 2018).

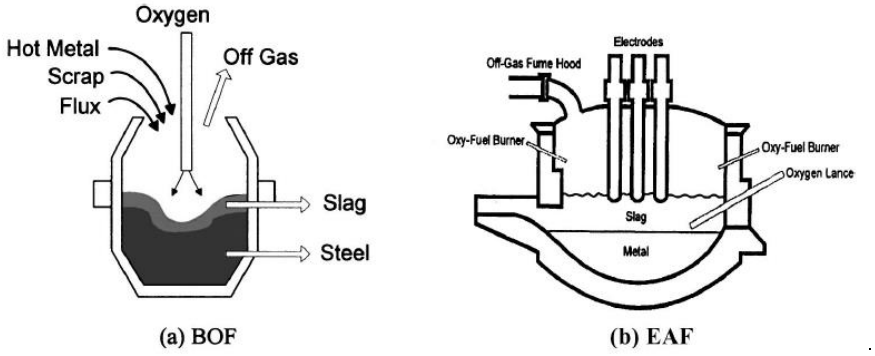

Figure 2.10. Schematic illustration of BOF and EAF process (Shi, 2004).

2.4 Foundry process

In a foundry process the furnace is used to bring the metal at the melting temperature to fill the forms to make the required object *(Figures 2.11 and 2.12)*.

In this case, to obtain the final product, it has been used an induction furnace, which mechanism is based on the relation between the magnetic and the electric field. The electric resistance of a conductive material is very low and so the energy dissipated by the Joule effect is high: the material to be melted acts as the secondary circuit, generating enough heat to bring the material to fusion.

An induction furnace is composed of: a copper coil to produce the inducing magnetic field, some flexible cables to bring power to the coil, a refractory which protects and shields the coil (often it has sensors to inform when the refractory is too thin and that can cause the formation of cracks which lead to dangerous episodes for the workers), some magnetic bars to avoid the excessive warming of the structure and a lid to hold the heat and also to treat the fumes.

Figures 2.11 and 2.12. Some photos of foundry production.

2.5 About steel slags

Steel slags represent the largest portion of by-products in an integrated steel mill, they are the product from the conversion of pig iron to steel in BOFs (Basic Oxygen Furnace) or the melting of scrap to make steel in an EAF (Electric Arc Furnace).

In this study we have used steel slags as mineral additions to cement. The formulations developed in this study are part of larger family of the "alkaline activated binders". In this case the alkaline activation is given by clinker. These binders may include, besides the slags, raw materials like metakaolin, fly ash, marble powder and rice husk.

From the first metal refining in the electric arc furnace it is obtained a first category of slags: the black slags, as previously presented. Further ladle metal refining produces the "white slags", which have been used in this work. To alloy the steel, elements like chromium, vanadium and molybdenum are added. The main difference between black and white slag is the chemical composition: the first one is richer in iron and the second one, from a further refining and alloying of steel slag, is poor in iron and rich in calcium.

In the present work steel slags are considered as a cementing component although it is not the general approach to their utilization, and also as a way to reduce the CO_2 emissions, because the production of Portland cement involves large emissions of green-house gases and requires a large amount of energy.

The industrial slags are not often valorised taking full advantage of their properties, mostly these materials are considered a waste and not recycled, instead they can be re-used like a cementitious material.

With this intent we tried to use steel slags to replace partially the cement to make a material which has a good mechanical resistance and good chemical properties.

So far, no case of negative environmental impact by ferrous slag has been reported when slag was used strictly in accordance with the requirements of the relevant regulations.

The use of ferrous slag, crystalline or vitrified, as aggregates, instead of natural rocks, such as limestone or granite, not only saves the energy that may be required to mine natural aggregates, but also eliminates the negative impacts associated with mining such as effects on biodiversity or disruption of the landscape.

In the case of cement manufacture, the use of granulated blast furnace slag instead of clinker reduces the overall process CO_2 emissions because of fuel savings and avoidance of calcining and decomposing limestone or other calcareous materials.

If we see some statistics made by the German FEhS (Institute for Building Materials Research) it shows that CO2-emissions have been reduced by about 22 million tonnes in the cement industry (hence in the industry as a whole) in Europe since 2008, because of the use of 24 million tonnes of granulated blast furnace slag (Euroslag, 2018).

The reduction is equivalent to the Kyoto objective of countries like Belgium and The Netherlands together. Thus, blast furnace slag contributes positively to the sustainability of the whole European industry and in the fight against climate change (Euroslag, 2018).

These data are about blast furnace slag, obviously we aim at doing the same with steel slags. Some 2016 data about production and use of steel making slags (including EAF slags) can be seen below in *Figures 2.13 and 2.14*.

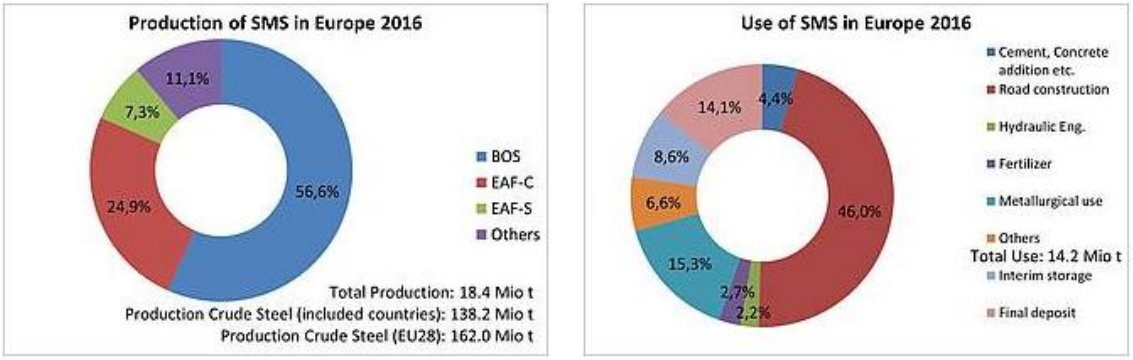

Figures 2.13 and 2.14. These figures show the production and the use of Steel Making Slags (SMS) in Europe in 2016. These data are, from a biennal survey conducted by Euroslag. (Euroslag, 2018).

2.5.1 Mineralogical properties of BOFs and EAFs

The chemical composition of steel slags *(Table 2.2)* depends on the steel which is produced. The slags mostly it consists of: CaO, SiO_2, MgO and FeO. Obviously, the proportions of these oxides vary based on the type of raw materials, the variety of steel produced, the type of furnace used and the conditions. The composition is driven by the process, so the variations are minor, because of process requirements.

The common mineral phases present in steel slags include minerals like olivine ($2MgO{\cdot}2FeO{\cdot}SiO_2$), merwinite ($3CaO{\cdot}MgO{\cdot}2SiO_2$), β and γ phases of C_2S ($2CaO{\cdot}SiO_2$), C_3S ($3CaO{\cdot}SiO_2$), C_4AF ($4CaO{\cdot}Al_2O_3{\cdot}FeO_3$), CaO (free lime), MgO, FeO and the RO phase (a solid solution of CaO-FeO-MgO-MnO).

Components	Basic oxygen furnace	Electric arc furnace (carbon steel)	Electric arc furnace (alloy/stainless)	Ladle
SiO_2	8–20	9–20	24–32	2–35
Al_2O_3	1–6	2–9	3.0–7.5	5–35
FeO	10–35	15–30	1–6	0.1–15
CaO	30–55	35–60	39–45	30–60
MgO	5–15	5–15	8–15	1–10
MnO	2–8	3–8	0.4–2	0–5
TiO_2	0.4–2	N/A[a]	N/A[a]	N/A[a]
S	0.05–0.15	0.08–0.2	0.1–0.3	0.1–1
P	0.2–2	0.01–0.25	0.01–0.07	0.1–0.4
Cr	0.1–0.5	0.1–1	0.1–20	0–0.5

[a]Not available.

Table 2.2. Chemical composition of steel slags (Shi, 2004).

The presence of C_3S and C_2S (the β polymorph) enhances the hydraulic properties of the steel slags. Also, these properties can be improved by the addition of proper activators, like alkali-activators which increase the strength of the material (Shi, 2004).

One of the main mineral phases in ladle slags is γ phase of C_2S, which is converted in the β phase during the cooling. This conversion, together with the long-term oxidation of metallic iron and Fe^{2+} to Fe^{3+}, causes an increase of the volume (about 10%) producing dusting due to the different crystal structures and densities.

The free lime (CaO) in steel slags comes from the precipitated lime from the molten slag and the residual free lime from the raw material used and the change of volume depends on the content of the residual lime (Shi, 2004).

Chapter 3

Characterization and materials

The materials involved in this work are three different products and they are all part of the family of steel slags called “white slags”:

- Slag A: ladle carbon steel
- Slag B: ladle stainless steel
- Slag C: foundry slag

In order to measure the chemical and physical properties of the materials and then their reactivity in different mixtures and formulations, the characterization techniques that have been used are:

- Fluorescence (XRF): to measure the elemental composition of the samples
- X-ray powder diffraction (XRD): to measure mineralogy and phase composition
- Scanning Electron Microscope (SEM): to measure texture, microstructure and elemental composition of individual grains
- Laser Granulometry: to measure particle size distribution, related to reactivity
- Calorimetry: to measure the hydraulic reactivity
- Mechanical tests: to measure the mechanical strength of slags different formulations

All the analyses introduced in this chapter (except for the mechanical tests) have been done at the *Department of Geoscience, University of Padua*.

3.1 X-ray fluorescence (XRF)

The spectrometer used is a WDS Philips PW2400, which is a sequential spectrometer equipped with a rhodium-anode X-ray tube, five crystal analysers (LiF220, LiF200, Ge, PE, TIAP), two detectors, three collimators and four filters. This instrument operates with the software SuperQ to do qualitative and quantitative analysis.

Using the x-ray fluorescence, the powder is hit by a primary x-radiation and each element emits a characteristic wavelength and intensity is proportional to abundance, after correction for a matrix effect. The abundance of every element is expressed in oxide percentage and the minor phases in part per million (ppm).

3.1.1 Sample preparation

In order to do a semi-quantitative analysis, a pellet has been prepared for each sample, using 3 grams of material to make each pellet (a pellet has been prepared and not a pearl, because there was the possibility to have some volatiles which would have been lost in process of making a pearl).

The sample powder has been put it in a steel cylinder, pressed with a plunger and then it has been added a powder mixture of wax/boric acid with a 1/3 ratio to build a “sleeve” on the edge of the sample (boron and carbon are not measured in XRF).

In the following step the powder has been pressed with a pressure of 6 tonnes, and the pill extracted from the press was ready to be analysed.

3.2 X-ray powder diffraction (XRD)

The diffractometer used is a PANalytical X'Pert PRO, using a Bragg-Brentano parafocusing geometry, equipped with a cobalt-anode X-ray tube (40 kV, 40mA) and a X'Celerator detector.

The X-ray powder diffraction pattern (XRD) has been used to investigate the mineralogic composition of the steel slags by doing a qualitative analysis or a semi-quantitative one with the use of the Rietveld method. The same procedure has been used to investigate the mineralogy of the hydration products.

3.2.1 Sample preparation

It is essential to carefully prepare the sample because the quality of the diffractogram depends heavily on the preparation of the sample.

The important thing about the sample preparation is the random distribution of the powder: the powder crystallites must be oriented in every direction randomly. The ideal sample would have an infinite number of crystallites organized in a random number of different orientations.

In order to do a quantitative analysis, it has been added 20% of zincite (ZnO) to the grinded sample, as an internal standard to calibrate for the matrix effect.

For the *slag A* we had two sizes of the material: the coarser one *(Figure 3.1)* had grains very different from each other (different for size, colour and shape), some magnetic parts and also some smaller grains. On the contrary, the other one was just really a fine light-brown powder.

Figure 3.1. The coarser part of the slag A before it has been separated from the magnetic part and grinded.

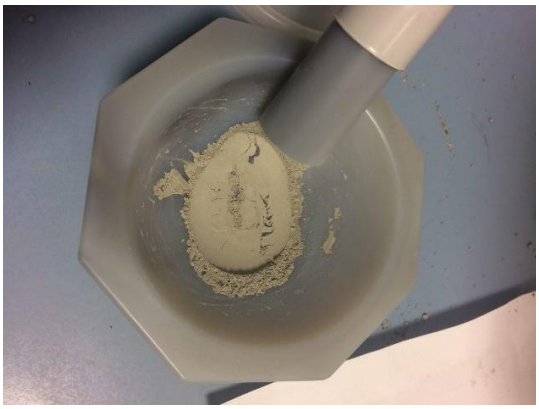

Figure 3.2. Slag A after the grinding with the agate mortar.

The samples have been prepared for the XRD diffraction analysis in different ways: for the first one it has been used a magnet to separate the magnetic parts; for the smaller grains, instead, it has been only used the agate mortar. Both the samples, grinded, had the same light-brown colour *(Figure 3.2).*

For the other two steel slags samples, *slags B and C*, it has been used the fraction passing a 63µm sieve and a vibrating screen to separate the >63µm part and the <63µm part.

For both the steel slags it has been used the <63µm part for the diffraction analysis, because the >63µm parts had magnetic grains. The colour between the two samples was very different: the *slag B (Figure 3.3)* is dark grey/black (due to the large presence of iron), *slag C (Figure 3.4)* is light brown.

The data have been analysed with the software programs High Score Plus and Topas.

Figure 3.3. The slag B (ladle stainless slag) as it is.

Figure 3.4. The slag C (foundry slag) as it is.

3.2.2 Quantitative analysis of hydration products

The samples have been micronized after the selected curing time (when the hydration process stopped). To perform a quantitative analysis the new phases formed have been analysed with an internal standard (20% of zincite).

3.3 Scanning Electron Microscope (SEM)

The SEM used is a CamScan MX3000, equipped with an EDAX energy dispersive spectrometer (20kV), with beam and aperture currents (20mA and 300nA respectively). The instrument uses a filament of lanthanum hexaboride (LaB_6) as the beam source.

The scanning electron microscope produces images by scanning the surface with a focused beam of electrons. It has been used to study the surface topography and the chemical composition of the samples using the Back Scattered Electrons (BSE) and the Secondary Electrons (SE).

The BSE are the product of the elastic interaction between electrons and atoms: these collisions cause a change of the electrons trajectories. They permit to differentiate the phases and to generate images which contain information on the sample composition. In addition, these kinds of images can give important information about crystallography and the magnetic field of the sample.

The SE have a minor energy compared to the BSE, because they are the result of the nonelastic interaction between the primary electron beam and the sample, they are useful to study the surface topography of the sample.

3.3.1 Sample preparation

The samples have been prepared with an epoxy with a sample/epoxy ratio of 10/3, they have been mixed together, put in a vacuum-sealed tube and then in the oven at 40°C for 12 hours.

Subsequently, they have been polished *(Figure 3.5)*, and thin sections have been made *(Figure 3.6)*. Finally, they have been polished to make the surface perfectly plane.

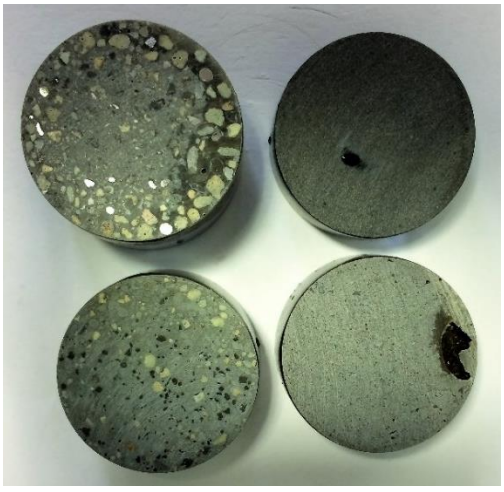

Figure 3.5. Capsules of the samples from which the thin sections were made.

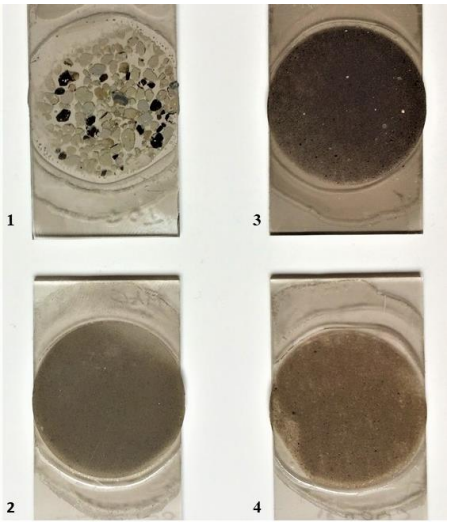

Figure 3.6. Thin sections of the samples ready to be analysed:

Number 1 and 2: slag A (as it is and only powder without the magnetic part)

Number 3: slag B

Number 4: slag C

3.4 Laser granulometry

The granulometer used is a Bettersizer SD (Dry), a particle size distribution analyser that adopts the Venturi dispersing effect.

Size and size distribution influence the handling, storage and domain of use of a powder. Not only the size of a cement powder particle can influence the hydration kinetics of the cement but also the state of agglomeration has a strong influence on the rheology of a cement paste (Scrivener, Snellings and Lothenbach, 2016).
The principle of a laser granulometer is based on the light scattering of particles of a given size and of the angular dependence of scattering as a function of particle size. Big particles scatter light on a narrow forward angle and with high intensity, vice versa small particles scatter on wider angles with low intensity.

The granulometric distribution is calculated by modelling the sample scattering through mathematical models.

The diffraction is described by two models: Fraunhofer and Mie. The Mie Theory, which is the one that has been used, is based on the electric field Maxwell's equations. A laser granulometer is composed of a laser source, a cell and a detector, the material is scattered as a dry powder dispersed through the Venturi's effect: the air jet smashes the material which is transported in front of the lens. Basically, the process is like an aerosol.

3.5 Calorimetry

Calorimetry comprises a set of techniques to measure the heat evolved or absorbed during chemical reactions, changes of state or other chemical processes, to determine the specific heat, thermal capacity and the latent heat.

The calorimetry system we used is constituted by a cup with a closing lid to prevent evaporation and isolated with a Styrofoam insulation. It is a semi-adiabatic calorimeter: the heat flux that goes from the calorimeter cell to the environment is constant. The heat exchange coefficient of the cell has been calibrated and the heat flux and hydration heat are expressed respectively in (W/g) and (J/g).

With this system we measured the hydration heat evolved during the setting of our hydraulic binders' formulations.

3.6 Mechanical Strength

Mechanical strength is a mechanical property which describes the maximum stress a material can support before the collapse. The strength of a composite material depends on many factors, such as porosity, microstructure (crystal intertwining) and surface cohesion.

About legislation, the norm considered for the cements classification is the *EN 197-1*, which classifies types and mechanical strengths of all the cements used in the European Union (described earlier, see *Chapter 2.2.3*). For the preparation of the specimens with mortar the norm considered is the *EN 196-1* (EN-196, Methods of testing and Cement, 2005), which controls dimensions, compositions and the conservation methods of the specimens.

3.6.1 Sample preparation

To measure the mechanical strength of the samples, different formulations with the three steel slags have been prepared, to measure how each slag behaves with the presence of gypsum and different quantities of the other components.

We have done two different types of tests: one has been done with paste mixtures and the other with mortar mixtures (only on a few samples, to compare the result with paste).

The materials used for the different formulations are:

- the three slags (A, B, C)
- cement 52.5R
- blast furnace slag Ecocem (D_{50} = 11.37)
- gypsum
- fly ash
- standard sand (for mortar formulations only)

For the paste formulations, the samples have been prepared and mixed, put in Teflon formworks of dimensions 15x15x60 mm^3 with a binder/water ratio of 0.5, then hit 30 times with a jolting apparatus. The day after they had been extracted from the moulds and immersed in water to cure the required time.

For the mortar formulations, the preparation was different compared to the one explained before. Steel formworks and a digital mortar mixer have been used. We have also prepared the small 15x15x60 mm^3 specimens with the mortar, to compare the two specimen dimensions (for the mortar formulations, the mixtures have been done at the *Department of Civil, Building and Ambiental Engineering (DICEA) at the University of Padua)*. The samples have been cured in water for 28 days, in a curing cabinet following the *EN-196-1* norm (EN-196 Methods of testing and Cement, 2005).

At the 28^{th} day the specimen dimensions and weight have been measured to deduce the density of each specimen, before doing compression and splitting tests.

These tests have been done on three sample per formulation type, to obtain statistical data: if the variance is low it means that the data are good and solids, in the same formulation there are not big changes on their compressive or splitting results.

3.6.2 Splitting and compression tests

In this work, two types of mechanical tests have been done on the samples: splitting and compression tests. Our specimens have a brittle behaviour (like all hardened concrete, mortar or paste), it means that if we apply a stress, the material will have a failure peak, the initial state will not recover, and it will collapse. *(Figure 3.7).*

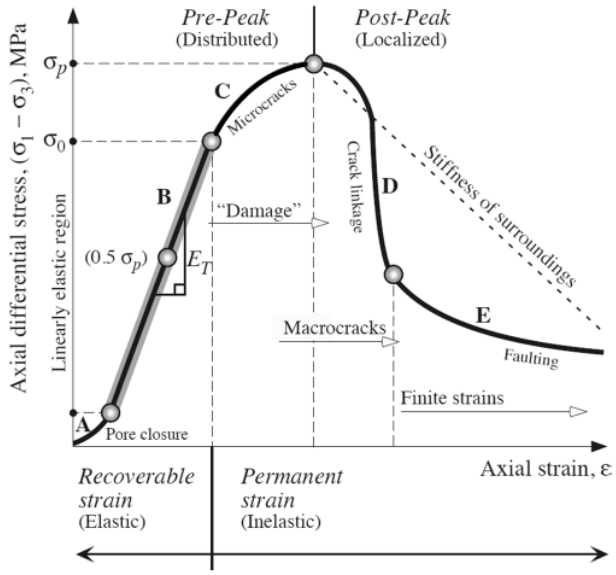

Figure 3.7. This graphic explains the behaviour of a brittle material. When the load is applied, the material deforms and, in the elastic regime, deformation is proportional to load (Hooke's law: $\sigma = E \cdot \varepsilon$; where E is the Young's modulus and ε is the strain). The pores start to close and some microcracks form (A). An increase of load produces a linear contractional strain (B). In the region C the slope decreases and so does the Young's modulus ($E = \frac{\sigma}{\varepsilon}$; where σ is the uniaxial stress and ε is the strain). The damage from now on is permanent, then there is the peak (material failure) and then the slope starts to decrease. The region D represents the "strain softening" deformation, lateral growth, propagation and linkage of microcracks arrays to form macrocracks. In closing, there is the "residual strength", where the slope becomes more linear (E) (Mazzoli, 2017).

The *splitting test* consists in the application of a uniaxial compression stress on a line, which generates a tensile stress in the perpendicular direction and brings the specimen to failure.
We measured three samples for each condition, thus we can determine the average value and of the standard deviation of the splitting and compressive strength.

For the *compressive test*, it is applied an increasing load on the face of the specimen, to bring it to failure.

The dimensions of the specimens must be inserted in the calculation to convert the splitting and compressive forces into pressures (strengths).

The splitting strength is calculated by a formula that considers the failure load *(Fs)* and the dimensions of the cross section *(A)* of the specimen:

$$fs = \frac{2Fs}{\pi \cdot A}$$

The compressive strength, instead, is calculated by considering the failure load *(Fc)* and both the base *(b)* of the specimen on which the compressive force acts and the width of the plate *(L)*:

$$fc = \frac{Fc}{b \cdot L}$$

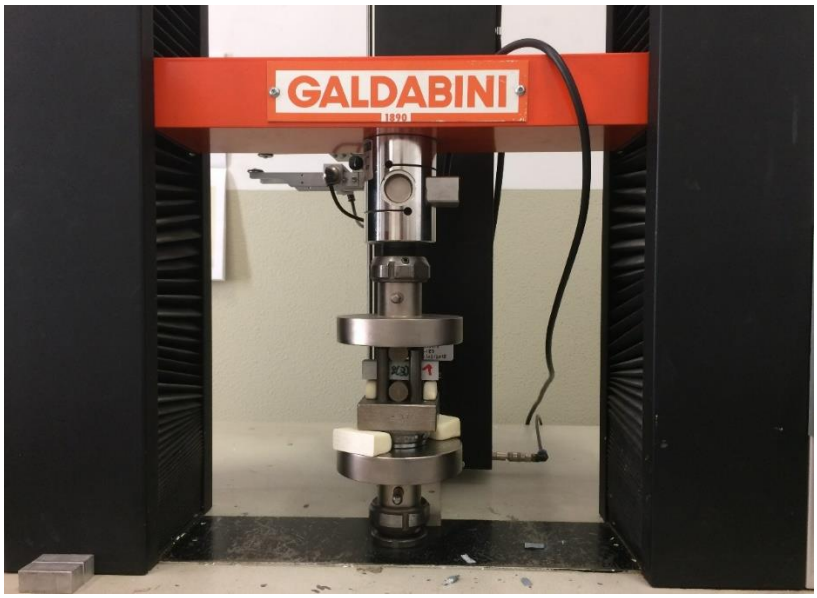

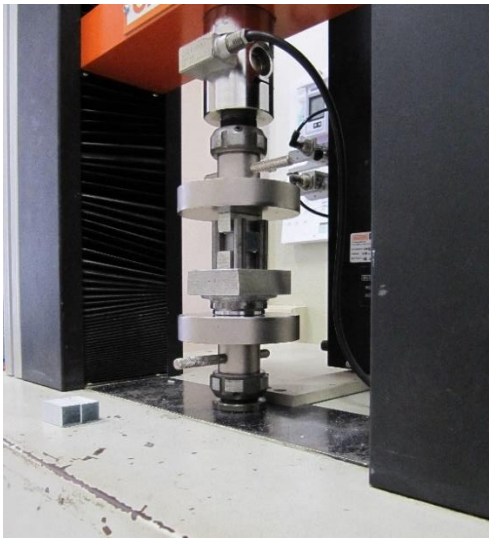

Figures 3.8, 3.9, 3.10. The press used for the mechanical tests: Galdabini Sun 60 Universal Machine, 600.000 N. The device used is a testing apparatus to measure small scale-samples of paste and mortars (designed and built by CIRCe, University of Padua, 2018). These mechanical tests have been done at the Department of Civil, Building and Ambiental Engineering (DICEA) at the University of Padua.

3.6.3 Experimental Design

The Experimental Design (DoE) is a statistical approach used to quantify the effect of experimental variables on a given property of the material. It allows the study of the effects of the different proportions of cementitious materials and additives on the binder paste. This method helps to interpret and to select the best combinations of factors to maximize the performance of the material. The factors are the variables, the coefficients describe a model which projects the effect on the product.

Specifically, in this work, it allows to estimate the best combinations of the different proportions of the components in the formulations in order to obtain the maximum mechanical performances.

The *regression model* permits to obtain the useful information to understand how much a factor is important in a system through the coefficients of the variables.

A large coefficient has a major influence on the behaviour of the system and the positivity, or the negativity, indicates the different effect on the variable of the answer.

The model built might not represent the system with accuracy: there might be interactions between variables not be considered in the model, which influence significantly the system behaviour.

To optimize a system we identify the important factors and for each one we fix the levels that need to be investigated: the number of the experiment is the combination of factors and levels of which $N°_{exp}$ = levels ^{factors} (Mangolini, 2018).

In this work by means of the Experimental Design approach we performed systematic changes on the slags contents and also on the contents of the other components to optimize performance.

This model has been the key to understand the best compositions to determinate the best mechanical strength for the three different slags.

Chapter 4

Results and discussion

4.1 X-ray fluorescence (XRF)

The chemical composition of the three slags, determined with the XRF analysis, is reported in *Table 4.1*.

We can make some important observations on the iron content: in the *slag B* it is very high (20.21% FeO) and the total percentage of the major elements in the *slags A* and *B* is above 100%, it means that iron is present in a reduced form (FeO and not Fe, since the metallic iron has been separated from the total sample).

Other features observed about the major elements abundance are the high magnesium content in *slag B* and the fact that *slag C* (foundry slag) is richer in SiO_2 than the other two.

About minor phases, we can notice the abundance in sulphur and zirconium in *slag A* and the high content in chromium and vanadium in *slag B.*

The chemical composition of the slags is reported in the ternary diagram in *Figure 4.1*, together with the existence ranges of Portland cement and blast furnace slag. We can also see from the diagram that *slags A* and *B* are richer in Al_2O_3, Fe_2O_3 compared to Portland cement.

	Chemical Abundance (Ox)	*Slag A*	*Slag B*	*Slag C*
%	SiO_2	20.14	25.6	44.67
	TiO_2	0.42	0.11	0.51
	Al_2O_3	17.37	11.37	7.73
	Fe_2O_3	3.92	20.21	3.46
	MnO	0.49	2.43	0.45
	MgO	6.75	2.83	2.27
	CaO	51.2	42.23	35.75
	Na_2O	0.11	0	0.5
	K_2O	0.04	0.02	0.61
	P_2O_5	0	0.1	0.04
	Tot major elements	**100.44**	**104.90**	**95.99**
ppm	S	16532	731	4380
	V	26	127	7
	Cr	1013	13191	76
	Co	2	0	3
	Ni	19	13	22
	Cu	138	65	54
	Zn	25	71	632
	Ga	1	8	0
	Rb	0	1	17
	Sr	280	138	520
	Y	9	2	29
	Zr	3131	73	240
	Nb	0	86	10
	Ba	641	88	553
	La	35	114	124

Ce	64	4	85
Nd	5	0	7
Pb	0	0	0
Th	14	6	7
U	4	3	8

Table 4.1. Results of XRF analysis. The major elements are expressed in percentage and the minor phases in ppm (part per million).

With these information, I was able to calculate the basicity of the three slags (*Table 4.2*), which is a marker of the potential hydraulic reactivity of the slags.

Slag	***SiO_2*** *(%)*	***CaO*** *(%)*	***Basicity***
A	*20.14*	*51.2*	*2.54*
B	*25.6*	*42.23*	*1.65*
C	*44.67*	*35.75*	*0.80*

Table 4.2. Basicity of the three different slags, calculated on the CaO/SiO_2 ratio.

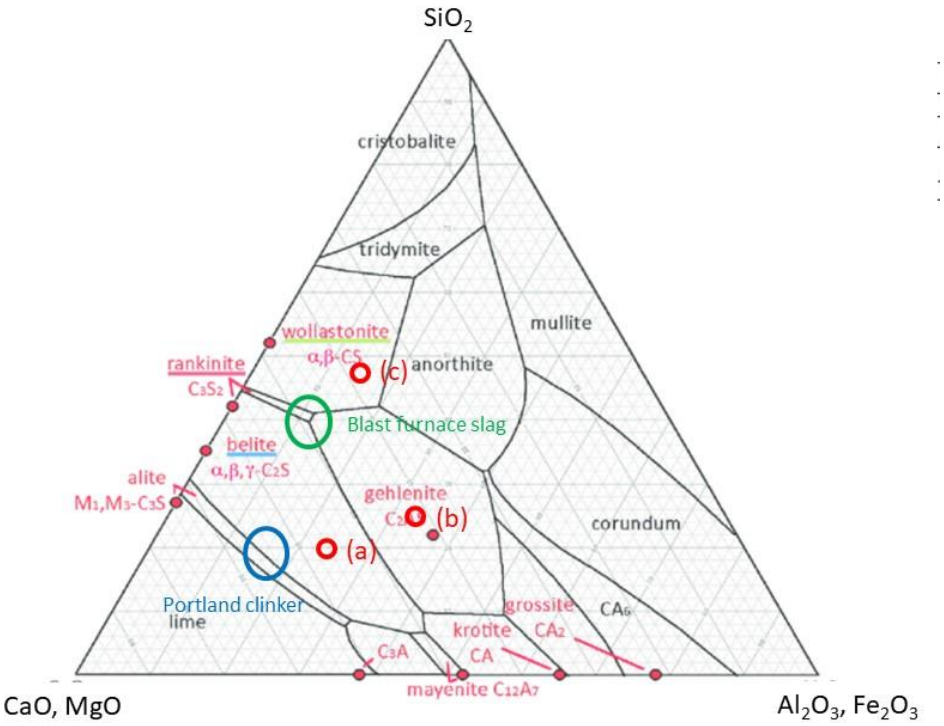

Figure 4.1. Ternary diagram of chemical composition of the three slags, based on SiO_2, Al_2O_3, Fe_2O_3, CaO, MgO abundance. a) ladle carbon steel, b) ladle stainless steel, c) foundry slag.

4.2 X-ray powder diffraction (XRD)

The x-ray powder diffraction analysis has been done in order to determinate the mineralogical composition of the three slags. In *Figure 4.2* the three diffractograms can be seen. Analyses of the different formulations after 2 (or 7) and 28 days

hydration were made to compare the growth of new phases (and the changes) in mineralogical composition, due to the hydration process.

Slag A has been analysed as it was. Conversely for the others two, the fractions passing and retained at the 63µm sieve have been analysed. For the *slag C* the two fractions were very similar, but for the *slag B* some differences can be observed in *Figure 4.3.*

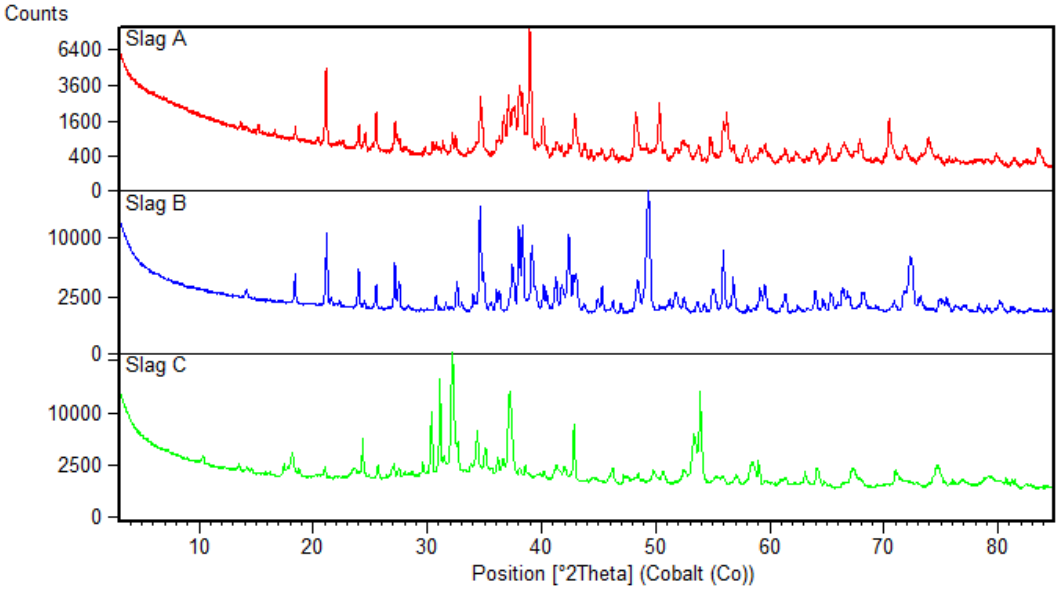

Figure 4.2. Comparison of XRD analysis of the three slags. Slag A has been analysed as it was, for slags B and C only the <63µm fraction has been considered.

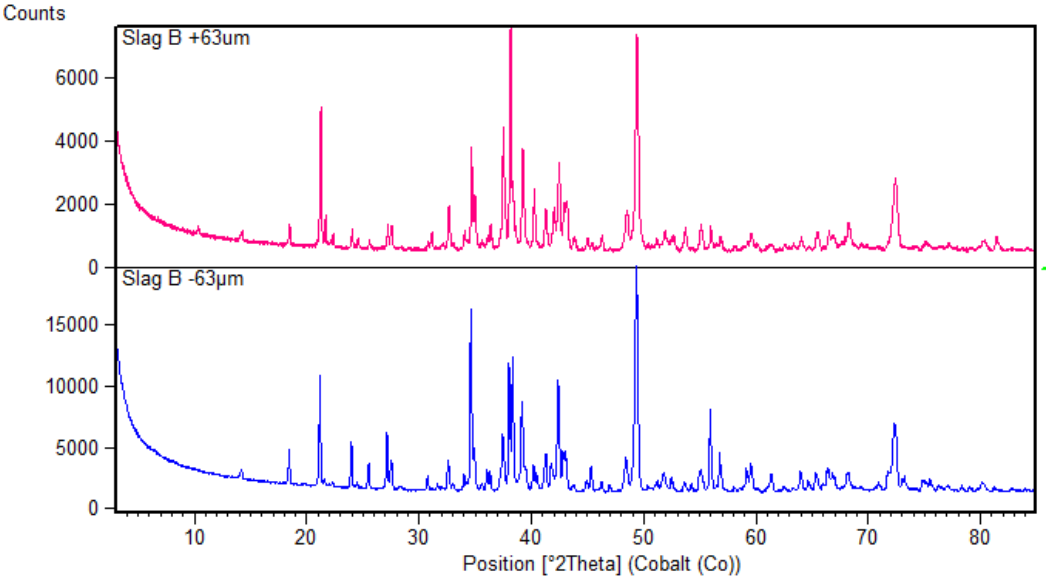

Figure 4.3. Differences between the >63µm (pink) and the >63µm (blue) fraction of slag B. Differences in the wustite (FeO) peaks at 49 2θ and 72 2θ can noticed: both peaks are lower in the <63 µm fraction, due to the magnetic separation.

The mineralogical composition of *slag A* is: mayenite ($Ca_{12}Al_{14}O_{33}$), larnite (Ca_2SiO_4, β-polymorph), calcium-olivine (Ca_2SiO_4, γ-C_2S), gehlenite ($Al_2Ca_2SiO_7$), merwinite ($Ca_3MgSi_2O_8$), quartz (SiO_2), periclase (MgO).

The mineralogical composition of *slag B* (<63µm fraction) is: calcium-olivine (Ca_2SiO_4, γ-C_2S), mayenite ($Ca_{12}Al_{14}O_{33}$), brownmillerite ($Ca_2(Al,Fe)2O_5$), larnite (Ca_2SiO_4, β-polymorph), chromium and iron spinels ($(Fe,Mg)(Cr,Al)_2O_4$), wustite (FeO), gehlenite ($Al_2Ca_2SiO_7$).

The mineralogical composition of *slag C* (<63µm fraction) is: quartz (SiO_2), calcite ($CaCO_3$), wollastonite ($CaSiO_3$), pseudowollastonite ($CaSiO_3$), cristobalite (SiO_2), larnite (Ca_2SiO_4, β-polymorph), akermanite ($Ca_2MgSi_2O_7$).

As we can see from *Table 4.3*, these slags, in particular *slag A* and the <63µm fraction of the *slag B*, contain a high quantity of larnite (Ca_2SiO_4, β-polymorph), so they are potentially hydraulic, but it is necessary to limit quick setting caused by the presence of mayenite.

Mineralogical phase	***Slag A (%)***	***Slag B (%)***	***Slag C (%)***
Larnite	30.1	13.5	7.8
Mayenite	16.6	21.7	/
Calcium-olivine	15.9	32	/
Calcite	/	/	15.3
Quartz	3.5	/	8.8
Cristobalite	/	/	1.5
Wollastonite	/	/	13.2
Pseudowollastonite	/	/	49.3
Wustite	/	32.7	/
Gehlenite	10.8	0.7	/
Brownmillerite	/	0.25	/
Merwinite	8.7	/	/
Fe and Cr spinels	/	2.3	/
Akermanite	/	/	4.5
Periclase	7.5	/	/
Perovskite	6.9	/	/

Table 4.3. Quantitative analysis of the mineralogical phases of the three steel slags, calculated by the Rietveld method. For the slags A and B only the <63μm fraction has been analysed. We can see that for slag A the main minerals are larnite, mayenite and calcium-olivine, for slag B are wustite, calcium-olivine and mayenite and for slag C are pseudowollastonite and calcite.

Note: about slag B, the main differences with the >63 μm fraction is the higher content in larnite, mayenite and spinels and the lower percentage of calcium-olivine. Also, the gehlenite is not present.

About the mineralogical and chemical composition of *slag A:*it is rich in periclase (MgO), which can lead to expansive phenomena and it is rich in sulphides that give some green-blue colouring upon hydration.

Slag B is rich in wustite (FeO), which makes the magnetic separation operations problematic during sample grinding: this operation may eliminate an important part of wustite which can carry, for the agglomeration effect, other oxides potentially reactive. Due to this problem, the magnetic separation during grinding must be avoided.

This slag is also rich in chromium and iron spinels ($(Fe,Mg)(Cr,Al)_2O_4$). The leaching behaviour of chromium must be controlled in order to assure its environmental compatibility.

Slags A and *B* are rich in mayenite ($Ca_{12}Al_{14}O_{33}$) and so they are rapidly reactive with water and show quick setting phenomena.

Slag C, which is different from the other because it comes from foundry production, has less hydraulic and pozzolanic phases and a low basicity index, so it is the less reactive of the three. On the other hand, this slag has does not have the quick-setting and dimensional instability problems shown by the other two.

4.2.1 XRD of hydration products

The hydration phases formed after 2, 7 and 28 days of hydration have been analysed by diffraction, with an internal standard (20% of zincite) to determine the amorphous fraction.

Some formulations analysed at 2 (or 7) days show the presence of hydration phases that in the 28 days hydration disappear or change to other minerals, due to the longer exposition to hydration process (*slags A* and *B*).

On the contrary, some formulations with *slag C* show very minimal changes.

The main hydrated products formed are: portlandite $Ca(OH)_2$, monosulphate, ettringite ($Ca_6Al_2(SO_4)_3(OH)_{12}\cdot 26(H_2O)$) (which forms from when gypsum is added), hydrotalcite *(*$Mg_6Al_2CO_3(OH)_{16}\cdot 4(H_2O)$) (an Al-Mg hydrate phase), which coherently with the elemental chemical composition of *slags A* and *B.*

In the formulations with *slag A* (A3, A8 and A9), the hydration products formed are: portlandite, ettringite, hydrotalcite and monosulphate. If the contents in GBBS is high, hydrotalcite forms at 28 days hydration, if the contents in slag is high, monosulphate forms at 28 days hydration. In the formulations with gypsum, at 2 and 7 days hydration there is still gypsum, which disappears at 28 days hydration with the formation of ettringite.

In the formulations with *slag B* (B3, B8 and B9), the hydration products formed are: portlandite, ettringite, hydrotalcite and monosulphate. If the contents in GBBS is high, hydrotalcite forms at 28 days hydration, if the contents in slag is high, monosulphate forms at 28 days hydration. In the formulations with gypsum, at 7 days hydration there is still gypsum, which disappears at 28 days hydration (formation of ettringite).

Slags A and *B* behave similarly.

In the formulations with *slag C* (C1, C3 and C5), the hydration products formed are: portlandite, ettringite, Al-Mg carbonate hydrate phase, Ca-Al carbonate hydrate phase and Fe-Mg silicate hydrate phase.

In the formulations with gypsum, at 7 and 28 days hydration there is ettringite.

The results and diffractograms of the hydration phases can be seen in *Appendix A*. The compositions of the formulations are reported later in this chapter (*Chapter 4.6, Tables 4.5*, *4.6* and *4.7*.

4.3 Scanning Electron Microscope (SEM)

With the Scanning Electron Microscope, some representative BSE images of the bulk structure were collected for the three slags. Also, a qualitative analysis of the chemistry has been done and the spectra have been analysed, to analyse the chemical element(s) in specific areas of the sample.

4.3.2 BSE Images and EDS Spectra

Here, some images of *slags A, B, C* and some chemical analyses are reported as examples and references.

Other BSE images and EDS spectra with detailed chemistry can be seen in *Appendix B.*

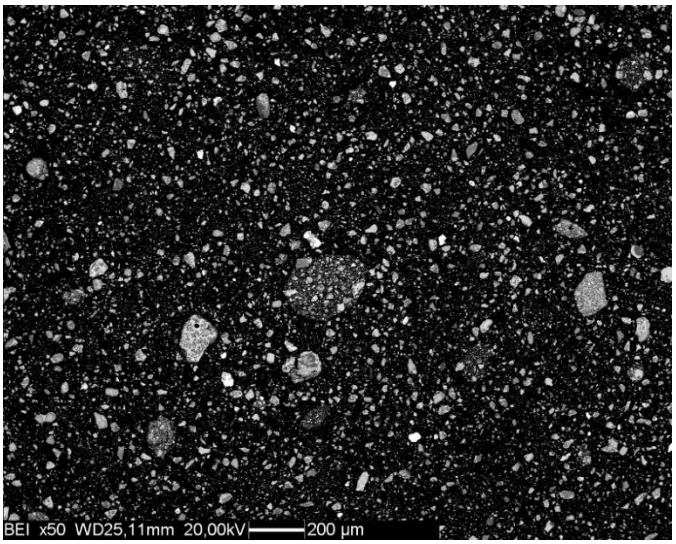

Figure 4.4. Panoramic image of slag A, BSE 50x.

In *slag A*, as we can see in *Figure 4.4*, the grains are not homogeneous and they are very small (they are the smallest of the three slags). Their dimensions are between 65 µm and <5 µm and some residual iron particles are present (white areas).

In the grains with spongy surface the presence of sulphur has been detected (see *figures 6.1B* and *6.3B* in *Appendix B*) by point EDS analysis.

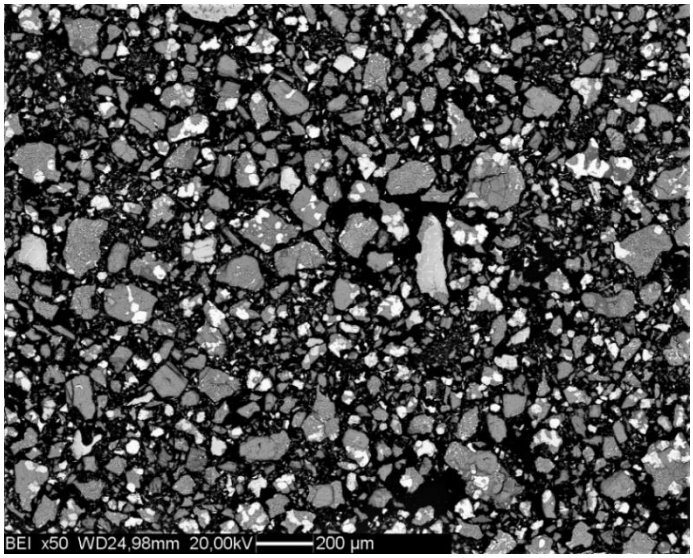

Figure 4.5. Panoramic image of slag B, BSE 50x.

In *slag B* the grains are quite homogeneous, with grain dimensions between 250 µm and <10 µm.

Note: in this slag, we observed with the naked eye some white popups, which can be visible at 2x magnification (in the form of little hilly white forms).

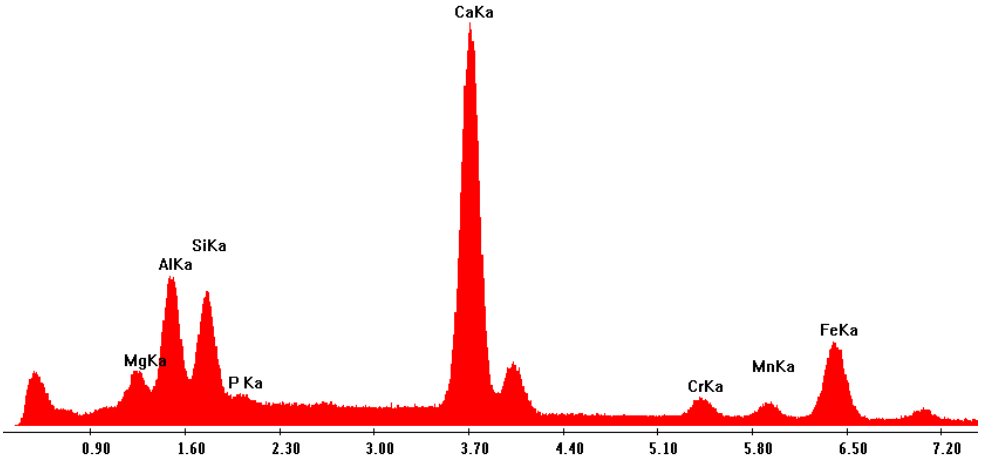

Figure 4.6. Panoramic of slag B chemistry.

As we can see in *Figure 4.6*, the major element is calcium (presence of calcium-olivine, larnite, brownmillerite, mayenite, gehlenite). Also, aluminium is quite abundant (from mayenite, brownmillerite, gehlenite and the Fe-Cr spinels), silica and iron (spinels, brownmillerite and wustite).

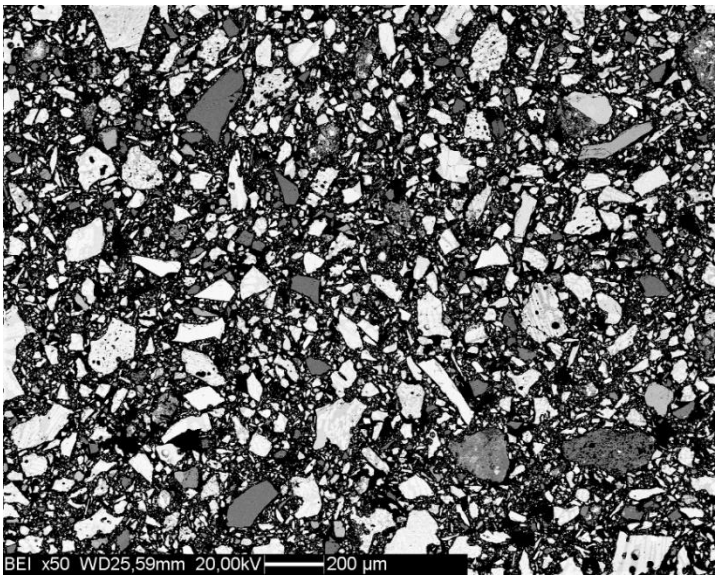

Figure 4.7. *Panoramic image of slag C, BSE 50x.*

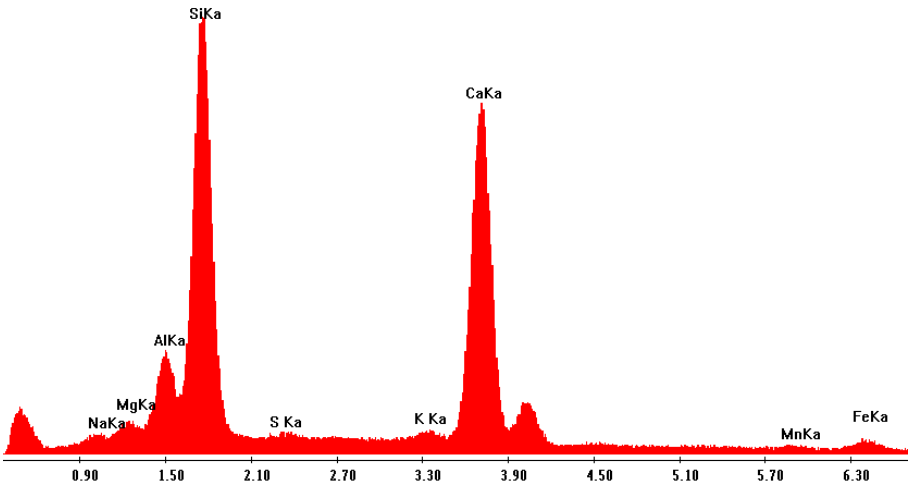

Figure 4.8. Panoramic of slag C chemistry.

In *slag C* as we can see in *Figure 4.8*, the major elements are silica and calcium because almost all the mineralogical phases of this slag are based on these two elements (quartz, calcite, wollastonite, pseudowollastonite, cristobalite, larnite).

4.4 Calorimetry

The calorimetry analysis has been done to see how the systems behave and react, to sketch out the reactivity of the systems in order to determine if the they were too reactive and showed quick setting. With this information we were able to choose the additions necessary to limit the activity of the materials.

The calorimetric measurements have been done with the formulations reported in *Table 4.4.*

The reactivity of each steel slag has been measured in a blend with 50% CEM I Portland cement and in a blend with 50% of a mixture composed of 50% CEM I and 50% blast furnace slag Ecocem 10µm.

The *slag A* is finer, and it has been used as such, while the others are coarser, and to avoid any bias of the data because of the different particle size the <63μm fraction has been used. The water /binder ratio is 0.5.

These formulations have been chosen to evaluate the reactivity of the steel slags with an alkaline activation brought up by Portland cement, and to evaluate the synergies between steel slags and blast furnace slag (Shi, 2004).

With the intent to control early setting and alkaline activation gypsum ($CaSiO_4 \cdot 2H_2O$) or sodium carbonate (Na_2CO_3) have been added in different quantities.

The mixtures had different workability, which influences the calorimetry results.

Slag A: A1 has a strong early peak and A2 is more liquid than the others, due to the absence of gypsum.

Slag B: B2 does not show quick setting.

Thermo-couple	***Cement*** *(%)*	***Blast Furnace Slag*** *(%)*	***Binder*** *(%)*	***Slag*** *(%)*	***Gypsum*** *(%)*	***Na_2CO_3*** *(%)*	***Fly ash*** *(%)*
A1	0	0	50	45	5	0	0
A2	0	0	50	45	0	5	0
A3	28	55	0	15	2	0	0
A4	28	50	0	15	2	0	5
B1	0	0	50	45	5	0	0
B2	0	0	50	45	0	5	0
B3	50	0	0	50	0	0	0
C1	0	0	50	45	5	0	0
C2	0	0	50	45	0	5	0
C3	50	0	0	50	0	0	0
C4	85	0	0	15	0	0	0
C5	80	0	0	15	5	0	0

Tab 4.4. Different composition of the formulations with the three slags (A, B, C), with a water/solid ratio of 0.5. The binder is composed of each steel slag and CEM I (50%) or CEM I plus blast furnace slag Ecocem 10µm (50%).

Here are reported in detail the different mixtures with their heat flow curves.

* CEM I 52,5 R cement and CEM III/A cement

As we can see below from *Figures 4.9* and *4.10*, calorimetry measures the heat flow curves and the reaction heat curves for the two cements. From these curves it is possible to measure the pozzolanic index for the blast furnace slag 10 µm, which is 0.41. It is calculated as the ratio between the heat evolved after 6 days of hydration by the CEM I and by the 50% blend of blast furnace slag and CEM I.

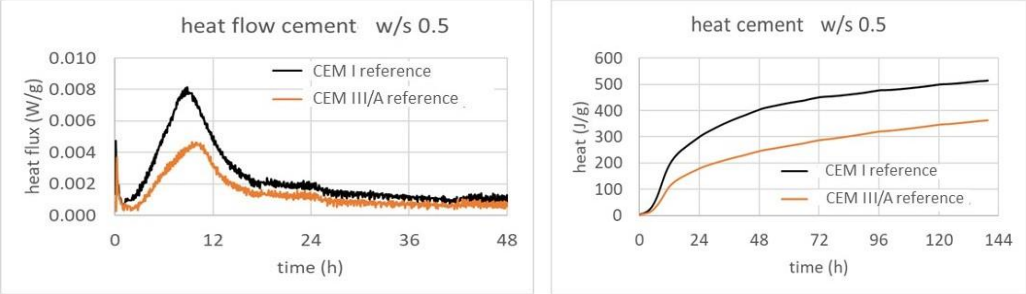

Figures. 4.9 and 4.10. Calorimetry results of the two cements used as reference to the three slags, with a 0.5 w/s ratio.

* Slags/CEM I and slag/CEM III mixtures

If we do a comparison between the three slags in a mixture with the CEM I 52.5 R, as we can see in *Figures 4.11* and *4.12*, *slags A* and *B* slags have a fast setting, whereas the *slag C* behaves like a good pozzolanic material, with a pozzolanic index of 0.29. Also, the *slag B* shows a hydration phenomenon at 48 hours.

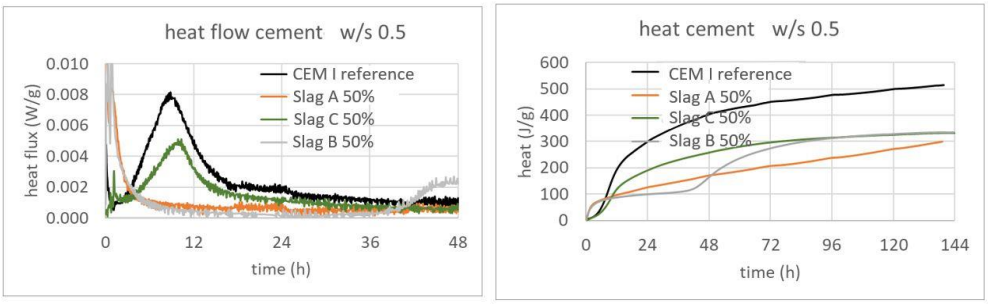

Figures 4.11 and 4.12. Calorimetry results of the three slags with CEM I as reference, with a 0.5 w/s ratio.

The comparison between the slags and the CEM III/A is different (*Figures 4.13* and *4.14)*: *slag B* shows again a quick setting, but the *slag A* has a very fast hydration at around one hour and another one at 18 hours.

The *slag A* slag has a pozzolanic index of 1.19, instead the *slag C* pozzolanic index is zero (it behaves like an inert). Also, the *slag B* shows a hydration phenomenon at 80 hours.

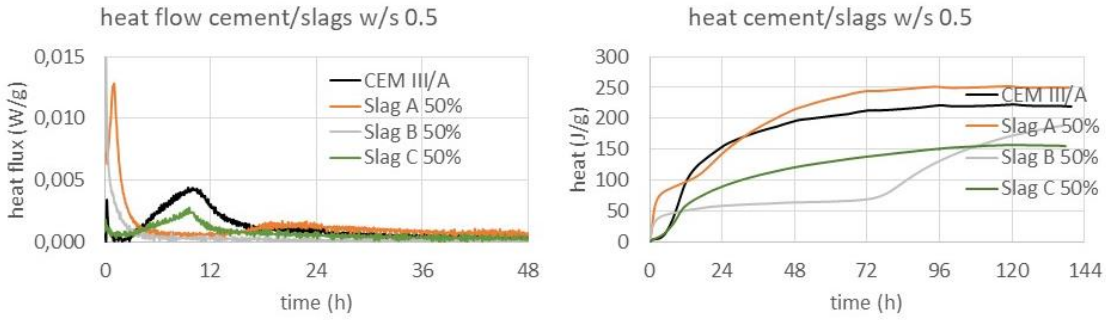

Figures 4.13 and 4.14. Calorimetry results of the three slags with CEM III as reference, with a 0.5 w/s ratio.

∗ Slags/CEM III/A with the addition of gypsum

In order to limit the quick setting phenomenon of *slags A* and *B*, it has been added some gypsum to the mixture. Here we can see in *Figures 4.15* and *4.16*, how the behaviour changes with 5% and 10% of gypsum.

Obviously, the addition of gypsum limits the quick setting.

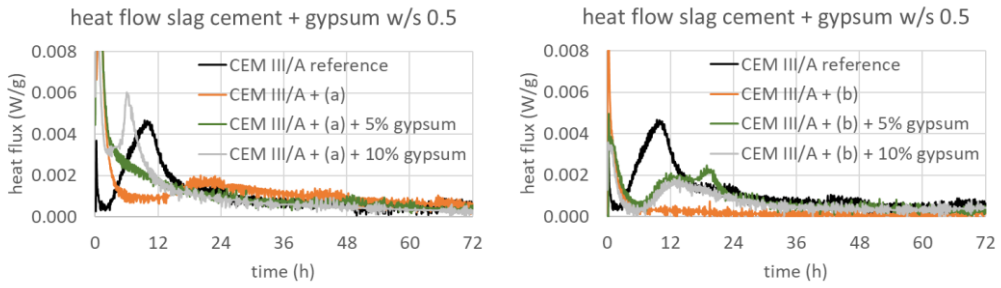

Figures 4.15 and 4.16. Calorimetry results of slags A and B with 5% and 10% gypsum addition, with a 0.5 w/s ratio.

* Slags/CEM III/A with the addition of Na_2CO_3

As we can see from *Figures 4.17 and 4.18*, we added Na_2CO_3 to find out if it acts like an activator for the slags and if it is good to limit the quick setting as the gypsum does. The presence of Na_2CO_3 in the *slag B* limits the quick setting, but in the other two it makes the situation worst. The *slag B* with 2% of Na_2CO_3 shows hydration at around 24 and 36 hours.

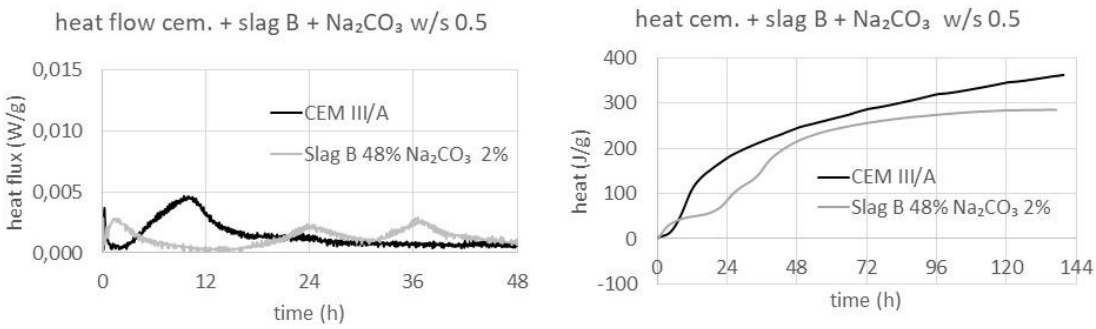

Figures 4.17 and 4.18. Calorimetry results of the addition of Na_2CO_3 (2%) in the slag B, with a 0.5 w/s ratio.

* Addition of fly ash to *slag A*

Looking at *Figures 4.19* and *4.20*, it has been added fly ash to *slag A* to favour the stratlingite formation ($Ca_2Al_2(SiO_2)(OH)_{10}\cdot 2.5(H_2O)$) and to accelerate setting while controlling early setting.

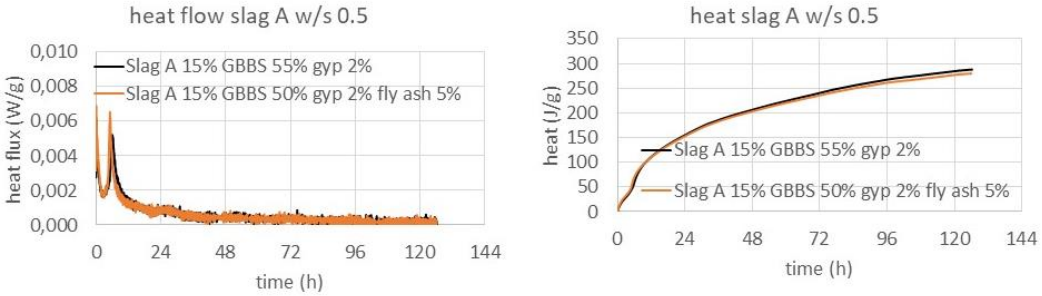

Figures 4.19 and 4.20. Calorimetry data of slag A with the addition of 5% of fly ash, with a 0.5 w/s ratio.

In *slag A*, we can see that, on increasing the quantity of gypsum, quick setting is reduced and so is the pozzolanic index (from 1.29 with no gypsum, to 1.01 with 5% of gypsum and 0.82 with 10%).

The addition of 5% of Na_2CO_3 makes quick setting worse and reduces the pozzolanic index from 1.29 to 0.23.

As regards *slag B*, we can see that the situation is different: on increasing the quantity of gypsum, quick setting is reduced. Also, the pozzolanic index is increased from 0.17 (with no gypsum) to 0.45 with 5% and 0.28 with 10% of gypsum.

The addition of Na_2CO_3 alleviates the quick setting (in particular the addiction of 2%) and increases the pozzolanic index from 0.17 to 0.57 with 2% and 0.63 with 5% of Na_2CO_3.

About *slag C*, the addition of gypsum increases the hydration heat and a contribute appears at 36 hours. The pozzolanic index increases from zero, with no gypsum, to 0.31 with 5% of gypsum.

For *slag A* and *B*, the data with blast furnace slag have been reported, while for *slag C* the data without should have been reported, since it only reduced the steel slag activity.

4.5 Laser granulometry

With the laser granulometer it has been possible to determine the particle size distribution of the slags, and to measure D_{50}, D_{10} and D_{90}.

These percentiles of the cumulative distribution are useful to describe the particle size distribution and they express the diameter for which 10%, 50% or 90% of the particles are smaller.

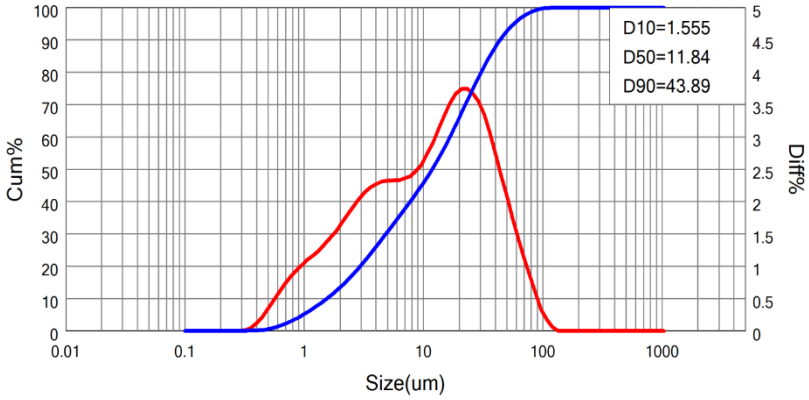

Diam um	Percent
0.500	0.55
1.000	5.15
2.000	13.41
5.000	30.69
10.00	45.75
20.00	65.99
45.00	90.51
75.00	98.16
100.0	99.73
200.0	100.00

Figure 4.21. Granulometry results of slag A.

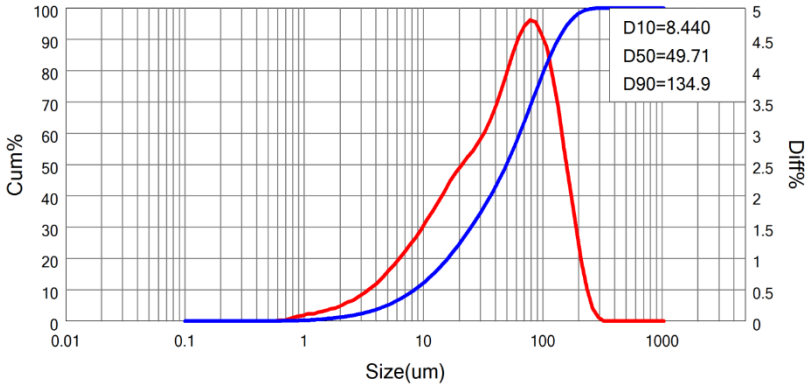

Diam um	Percent
1.000	0.21
2.000	1.19
5.000	5.05
10.00	12.18
20.00	24.72
45.00	46.52
75.00	66.60
100.0	79.10
200.0	98.35
300.0	100.00

Figure 4.22. Granulometry results of slag B.

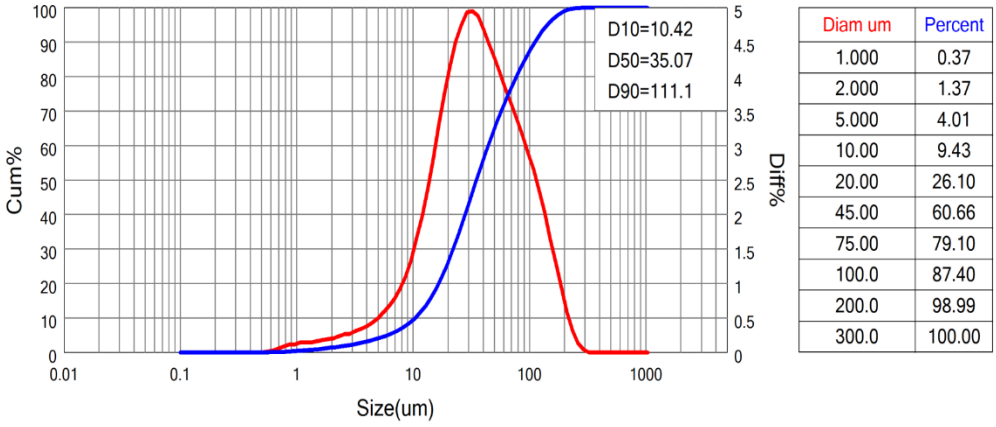

Diam um	Percent
1.000	0.37
2.000	1.37
5.000	4.01
10.00	9.43
20.00	26.10
45.00	60.66
75.00	79.10
100.0	87.40
200.0	98.99
300.0	100.00

Figure 4.23. Granulometry results of slag C.

We can see clearly that *slag A* is the finest one, with a value of D_{50}= 11.84. The other two slags have a D_{50} of 49.71 (*slag B*) and 35.07 (*slag C*).

These data are coherent with the calorimetry results, in fact the *slag A*, the finest of the three, is the most reactive (see Calorimetry, *Chapter 4.4*).

4.6 Mechanical Strength

The formulations used for the preparation of the specimens with the *slags A*, *B* and *C* are reported in *Table 4.5*.

During the preparation we observed that sample A4 showed quick setting (it contains no gypsum). On the contrary samples A6, A7 and A9 were liquid and showed bleeding.

Sample	***Cement*** *(%)*	***GBBS*** *(%)*	***Slag*** *(%)*	***Gypsum*** *(%)*
A1	32	18	50	0
A2	44.8	25.2	30	0
A3	17.5	32.5	50	0
A4	24.5	45.5	30	0
A5	32	18	35	15
A6	44.8	25.2	15	15
A7	17.5	32.5	35	15
A8	24.5	45.5	15	15
A9	29.7	30.3	32.5	7.5
B1	32	18	50	0
B2	44.8	25.2	30	0
B3	17.5	32.5	50	0
B4	24.5	45.5	30	0
B5	32	18	35	15
B6	44.8	25.2	15	15
B7	17.5	32.5	35	15
B8	24.5	45.5	15	15
B9	29.7	30.3	32.5	7.5
C1	50	0	50	0
C2	70	0	30	0
C3	50	0	45	5
C4	70	0	25	5
C5	60	0	37.5	2.5

Table 4.5. Table of the formulations with slag A, B and C used for the mechanical strength tests. The formulations with slag C do not include the blast furnace slag Ecocem 10µm.

The mechanical strength results of paste formulations are reported below, in *Table 4.6*:

Sample	***AVG Density (g/cm^3)***	***Splitting (N)***	***CoV σ_t (%)***	***Compression (N)***	***CoV σ_c (%)***
A1	1.80	618,79	7.35	4143,04	7.77
A2	1.86	707,38	10.62	5358,79	6.39
A3	1.80	707,58	10.08	4561,50	5.61
A4	1.82	639,5433	20.82	7281,42	3.77
A5	1.73	611,09	14.10	5770,21	4.44
A6	1.73	969,09	12.23	6158,54	10.49
A7	1.75	566,58	24.09	5407,38	4.25
A8	1.73	1001,88	23.74	5149,17	2.96
A9	1.78	572,59	14.24	6151,79	4.34

Table 4.6. Table of the density, splitting and compression results (with the respective variances) of mechanical tests on slag A.

Notes: sample A1 was inhomogeneous, sample A2 was not well compacted and sample A5 showed some lumps, due to the presence of gypsum not well dispersed *(Figures 4.24 and 4.25).*

Sample	*AVG Density (g/cm^3)*	*Splitting (N)*	*CoV σ_t (%)*	*Compression (N)*	*CoV σ_c (%)*
B1	1.82	573,34	9.49	3255,09	3.51
B2	1.83	664,08	11.82	6757,42	5.28
B3	1.82	528,00	14.19	4178,13	1.95
B4	1.85	621,54	17.34	6108,71	6.50
B5	1.63	781,71*	16.82	2236,13**	10.31
B6	1.75	792,09	7.38	4442,38	3.80
B7	1.80	782,75	15.15	3545,87	4.11
B8	1.73	833,71	7.20	4212,50	3.33
B9	1.74	616,75	8.38	4429,63	8.13

Table 4.7. Table of the density, splitting and compression results (with the respective variances) of mechanical tests on slag B.

Notes: in sample B5 (* and **) the result can't be considered because the samples were already fractured before the measurement because of expansion *(Figure 4.26)*.

Sample	*AVG Density (g/cm^3)*	*Splitting (N)*	*CoV σ_t (%)*	*Compression (N)*	*CoV σ_c (%)*
C1	1.74	639,54	4.50	7281,42	11.69
C2	1.75	611,09	2.91	5770,21	5.32
C3	1.65	969,09	20.33	6158,54	2.55
C4	1.69	566,58	3.95	5407,38	5.22
C5	1.69	1001,88	4.23	5149,17	8.00

Table 4.8. Table of the density, splitting and compression results (with the respective variances) of mechanical tests on slag C.

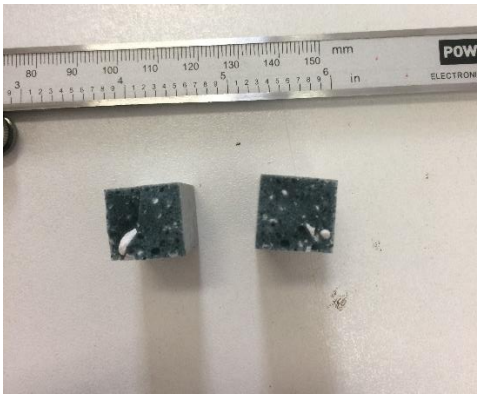

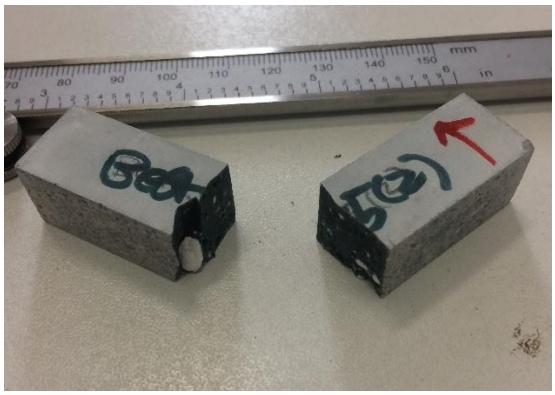

Figures 4.24 and 4.25. Lumps due to the gypsum presence in sample A5.

Figure 4.26. Fractures due to expansions in sample B5.

In *Table 4.9* are reported the different formulations for the mortar mixtures, which include the standard sand.

According to the norm EN 196-1, the standard mortar is prepared with:

- Standard sand (1350 grams)
- Cement or binder (450 grams)
- water/solid ratio of 0.5

These mortar formulations have also been used in the Teflon formworks, to compare the two specimens and to check if there are any strength differences due to the different dimensions.

Sample	***Cement*** *(%)*	***GBBS*** *(%)*	***Slag*** *(%)*	***Gypsum*** *(%)*
B1_M	22	33	40	5
C1_M	65	0	33	2
C2_M	48	0	50	2

Table 4.9. Table of the slags B and C for mortar formulations to do the mechanical strength tests.

The mechanical strength results of mortar formulations are reported below in *Table 4.10*.

Sample	*AGV Density (g/cm^3)*	*Splitting (N)*	*CoV σ_t (%)*	*Compression (N)*	*CoV σ_c (%)*
B1_M	2.21	8035.80	7.32	52947.67	2.11
C1_M	2.19	8664.71	9.03	53510.00	0.95
C2_M	2.19	7384.58	1.62	38617.67	3.71
B1_m	2.21	1429,17	9.43	6547,92	2.52
C1_m	2.09	1394,79	10.76	6830,71	2.79
C2_m	2.14	819,32	16.16	4820,42	3.05

Table 4.10. Table of the density, splitting and compressive strength results (with the respective covariances) of mechanical tests on mortar formulation on slags B and C.

M= tests done with steel formworks, 40x40x160mm; m= tests done with Teflon formworks, 15x15x60mm

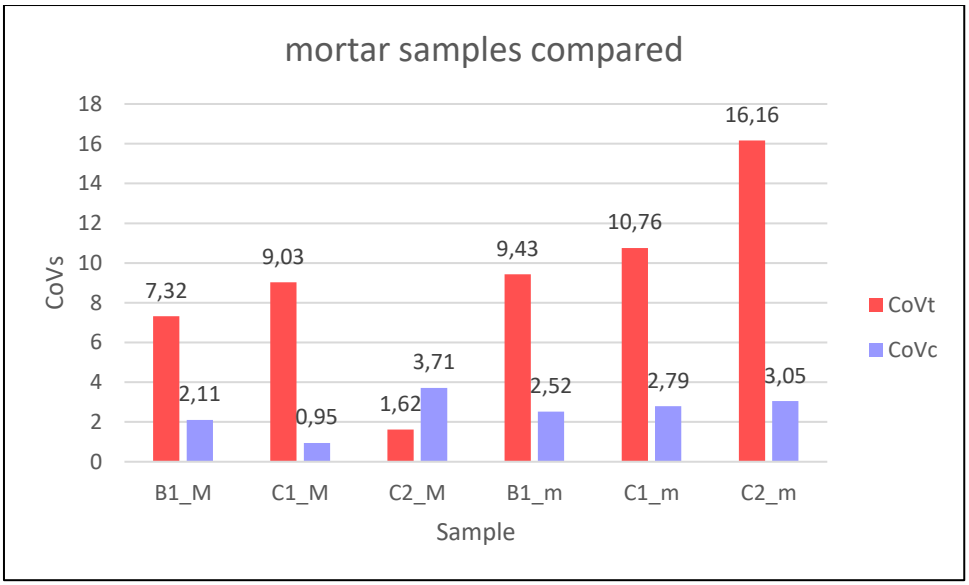

Figure 4.27. CoVt and CoVs of mortar formulations compared. The first three are the ones done with steel formworks, 40x40x160mm; the others three are the ones done with Teflon formworks, 15x15x60mm. The values are lower and the variance is larger.

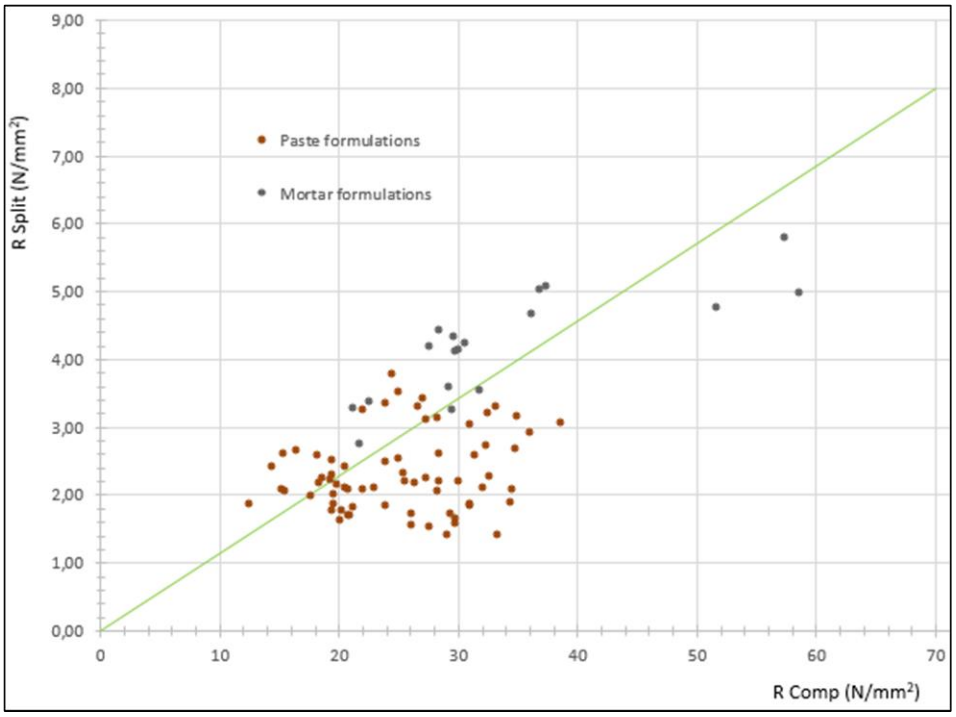

Figure 4.28. This graphic shows a comparison between paste and mortar formulations on their compression and splitting trends.

Considering the splitting and compression data obtained and the different formulations, it has been possible to determine through linear interpolation of the data the formulations to reach strengths of 32.5 and 42.5, utilizing systems with slag, GBBS and gypsum (for *slag A*) and slag and gypsum (for *slag C*).

Formulation	***Cement (%)***	***GBBS (%)***	***Slag (%)***	***Gypsum (%)***
Slag A_1	28	55	15	2
Slag A_2	28	50	15	2
Slag C_1	85	0	15	0
Slag C_2	80	0	15	5

Table 4.11. Final formulations in order to obtain mechanical strengths of 32.5 MPa and 42.5 MPa.

Chapter 5

Conclusions

Through the characterization and the mechanical tests made on the three steel slags, it has been possible to draw the following conclusions.

In this work we have analysed three different slags, two of them are from EAF process *(slags A and B)* and the other one is from foundry production *(slag C).*

Slags A and *B*, as we can see from calorimetry results, are very reactive, they have a high basicity index (2.54 and 1.65 respectively) and if they are mixed only with cement, result in a quick setting. This happens because they are particularly rich in mayenite ($Ca_{12}Al_{14}O_{33}$) and they also contain a high quantity of larnite (Ca_2SiO_4, β-polymorph). They are potentially hydraulic, but it is necessary to control the quick setting. They rapidly generate a high hydration heat flow, which is not desirable, so they must be mixed with something to slow down their reactivity. A good solution is to use blast furnace slag and gypsum which, when conveniently mixed, give coherent and useful reaction ranges.

As we can see from the granulometry results, *slag A* is the finest one, with a D_{50} of 11.84, and it is the most reactive also by virtue of this property.

Slag C, instead, is different from the other two because it comes from a different production process and, consequently it has a different mineralogical composition, constituted by minerals rich in calcium and silica. It has a low reactivity, less abundant hydraulic and pozzolanic phases and a low basicity index. It can be mixed to the cement as it is (it does not need the addition of the GBBS) and it does not create any problems, because it has no phases which lead to quick setting or expansive reactions.

The only negative thing about this product is the fact that a high quantity of slag in the formulation decreases the mechanical strength.

About mechanical strength data, they vary considerably according to the different formulations chosen.

The results obtained confirm that, with convenient quantities of slag, GBBS (for *slags A* and *B*) and gypsum, we are able to reach the strength classes of 32.5 MPa and 42.5 MPa.

Appendix A

Hydration phases XRD diffractograms

The formulations as reference can be seen on *Chapter 4.6, Table 4.5*.

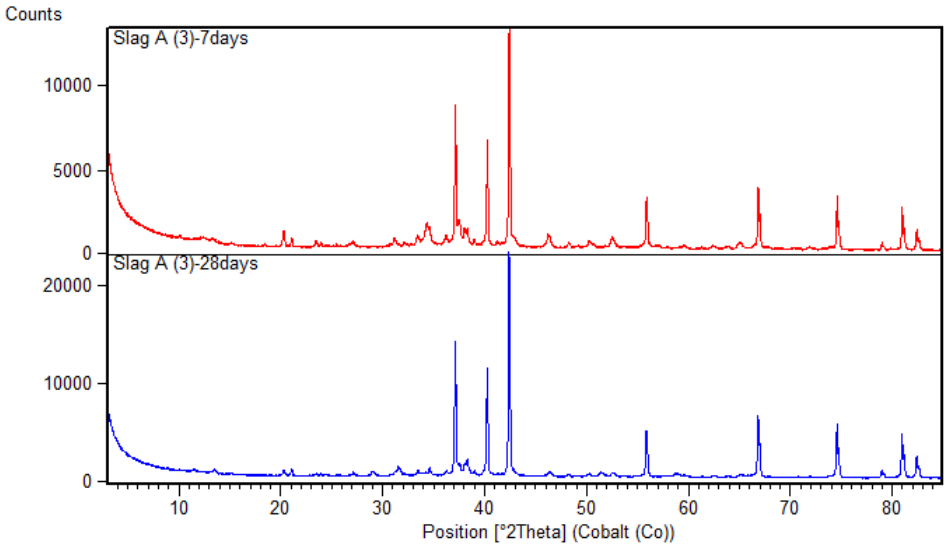

Figure 6.1A. Slag A, formulation 3.

There are no significant changes on hydration phases at 7 and 28 days.

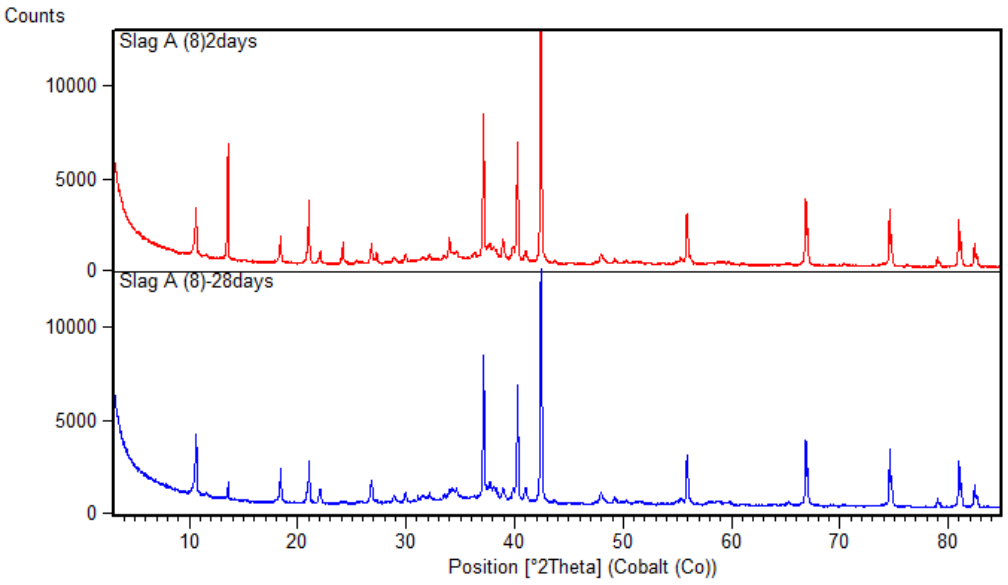

Figure 6.2A. Slag A, formulation 8.

The hydration phases at 2 and 28 days change a lot. The peak of gypsum at 13 2θ is a lot higher than the one in the 2 days hydration sample (the peak of gypsum at 24 2θ at 2 days can be seen, but not in the other diffractogram at 28 days; also, the peak of gypsum at 27 2θ can't be seen, but only the one at 26 2θ, which is the peak of ettringite). On the 28 days hydration we can see that gypsum decreases because it becomes ettringite, this can be noticed also at 34 2θ, where the peak of ettringite is higher in 28 days hydration. Another thing that can be seen is the formation of hydrotalcite ($Mg_6Al_2CO_3(OH)_{16}\cdot 4(H_2O)$), (13 2θ peak of hydrotalcite is seen on the 28 days but not in the 2days).

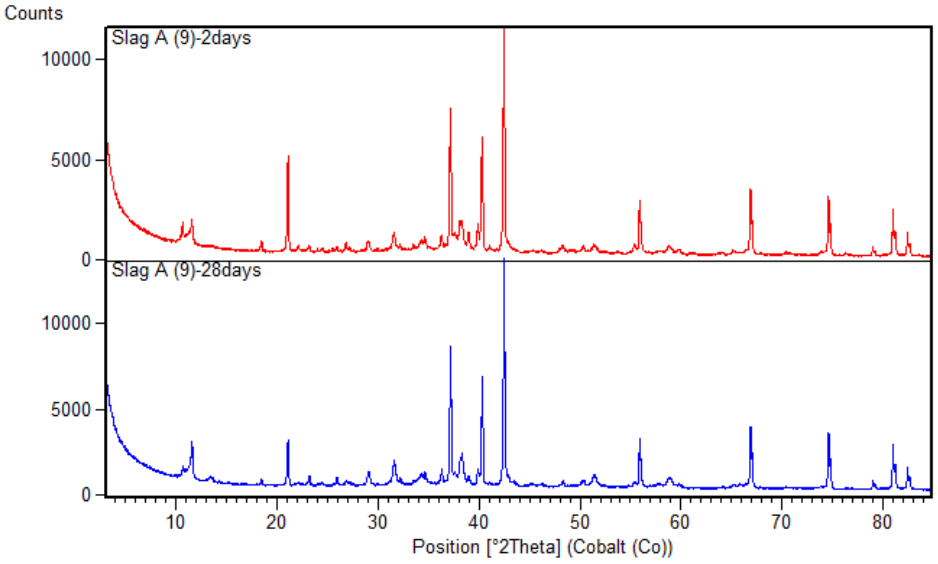

Figure 6.3A. Slag A, formulation 9.

The hydration phases at 2 and 28 days change a little bit. The ettringite peak at 10 2θ in the 2 days hydration can be seen well and it is lower in the 28 days hydration. The monosulphate peak at 11 2θ is higher in the 28 days hydration.

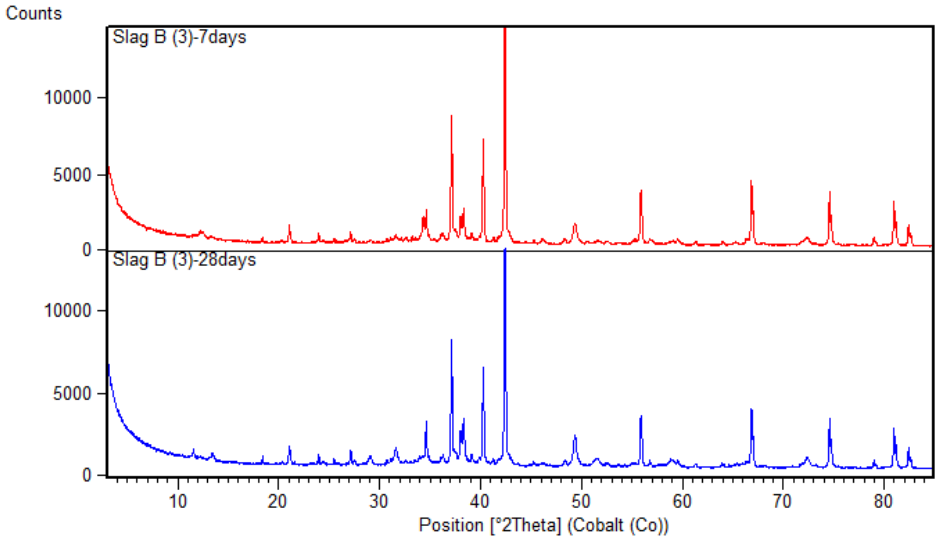

Figure 6.4A. Slag B, formulation 3. The hydration phases at 7 and 28 days change.

The intensity changes at 28 days hydration for these peaks:

- 24 2θ and 29 2θ, calcium-olivine: in the 7 days hydration the peak disappears (or it is lower)
- 31 2θ and 34 2θ, mayenite: in the 7 days the peak disappears (or it is lower).

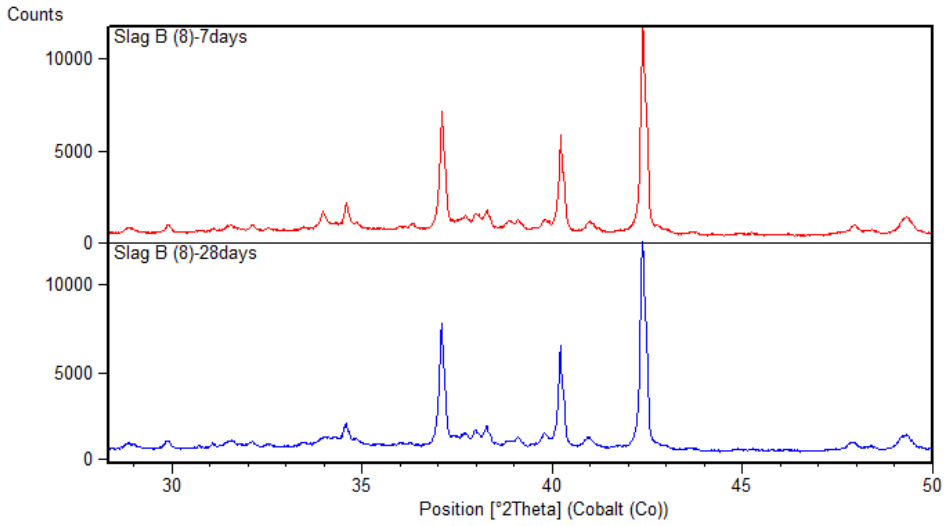

Figure 6.5A. Slag B, formulation 8.

The hydration phases at 7 and 28 days change. It can be clearly seen the peaks of gypsum at 13, 14 and 33 2θ, a phase that does not exist anymore at 28 days of hydration.

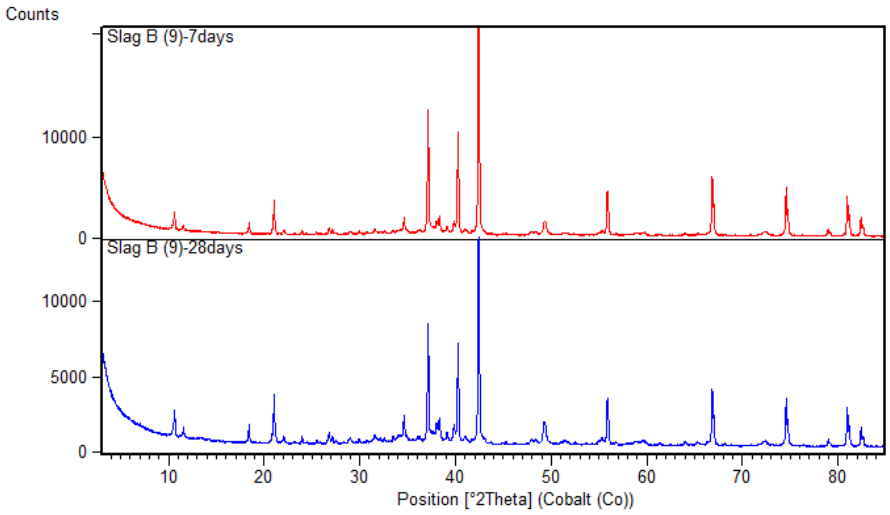

Figure 6.6A. Slag B, formulation 9.

The hydration phases at 7 and 28 days change a little. The peak of ettringite at the 18 2θ is higher in the 28 days hydration.

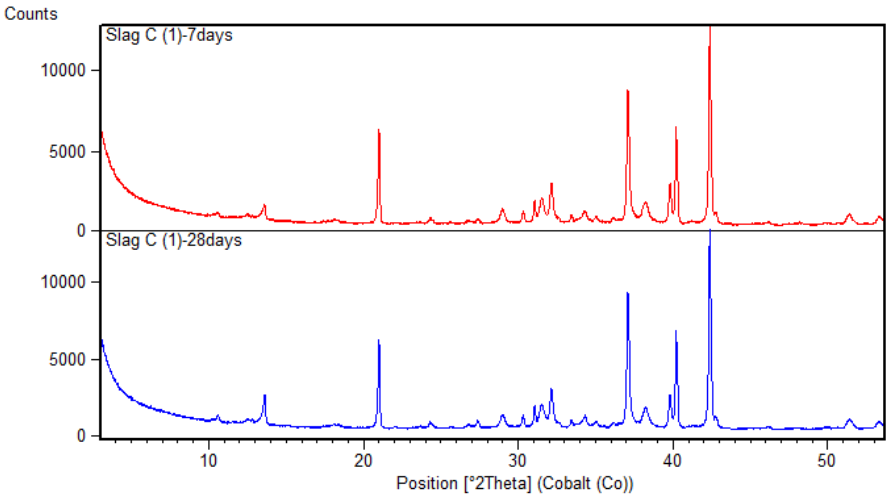

Figure 6.7A. Slag C, formulation 1.

The hydration phases at 7 and 28 days do not change, except for the intensity of peak 13 2θ, which in the 28 days is higher (it's an aluminium-magnesium hydrate carbonate phase).

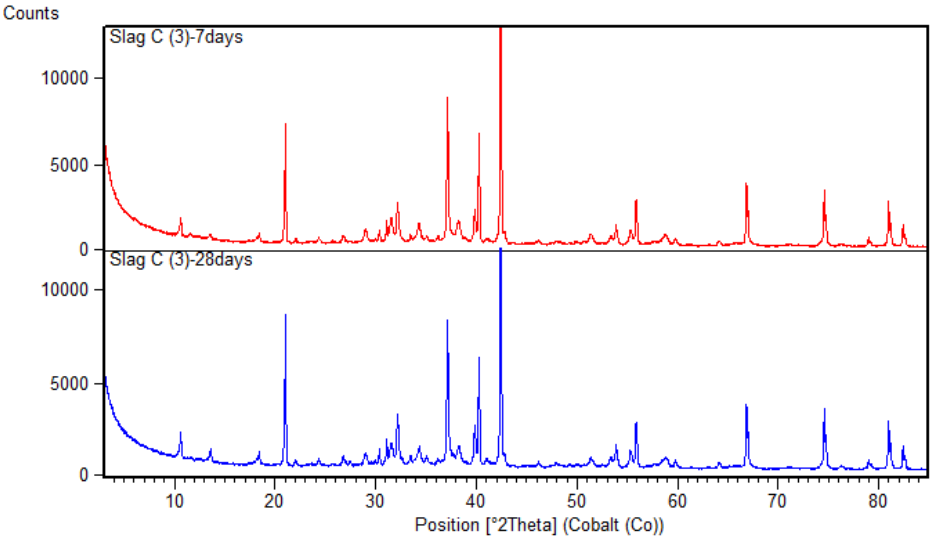

Figure 6.8A. Slag C, formulation 3.

The hydration phases at 7 and 28 days do not change, except for the intensity of a peak (21 2θ), which in the 28 days is higher (it's portlandite).

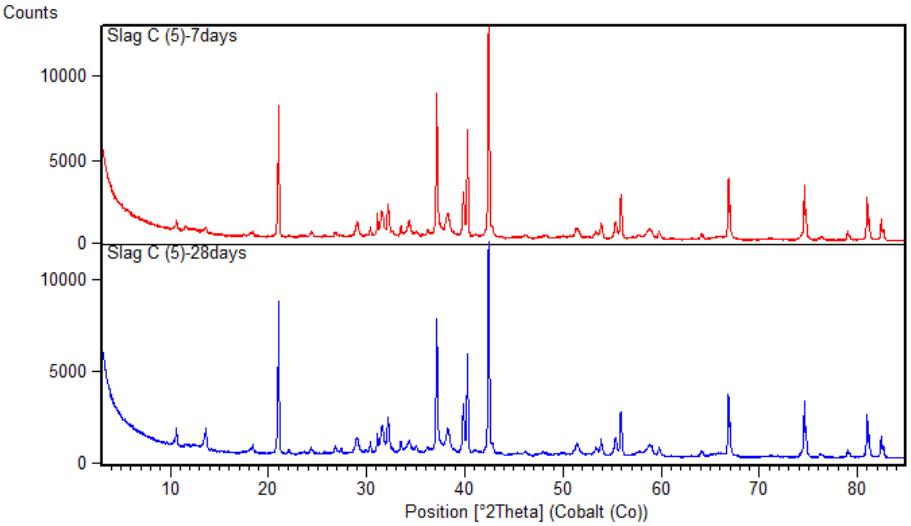

Figure 6.9A. Slag C, formulation 5.

The hydration phases at 7 and 28 days do not change much, except for the intensity of two peaks (10 2θ and 13 2θ), which in the 28 days are higher (ettringite and Al-Mg hydrate carbonate).

Appendix B

BSE Images and EDS Spectra (SEM)

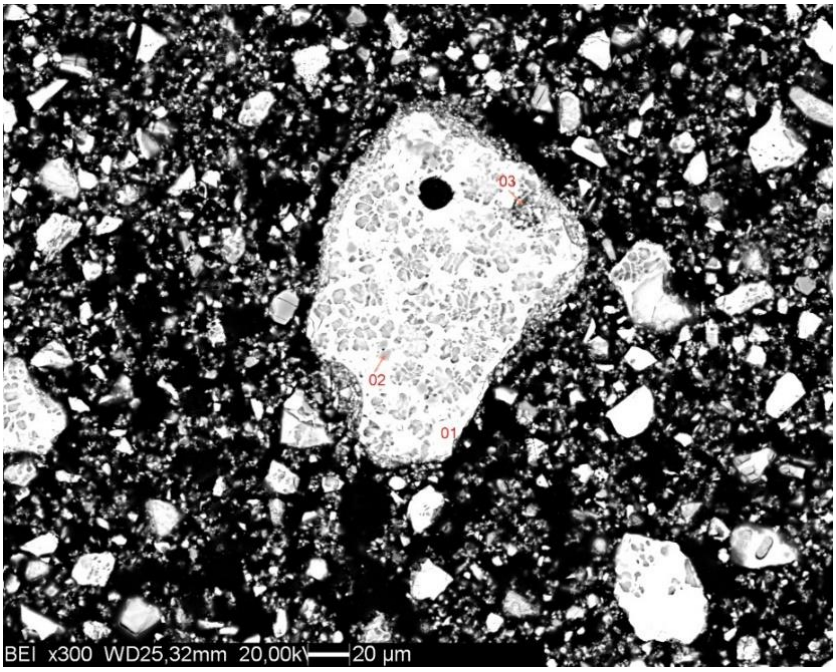

Figure 6.1B. Slag A, BSE 300x

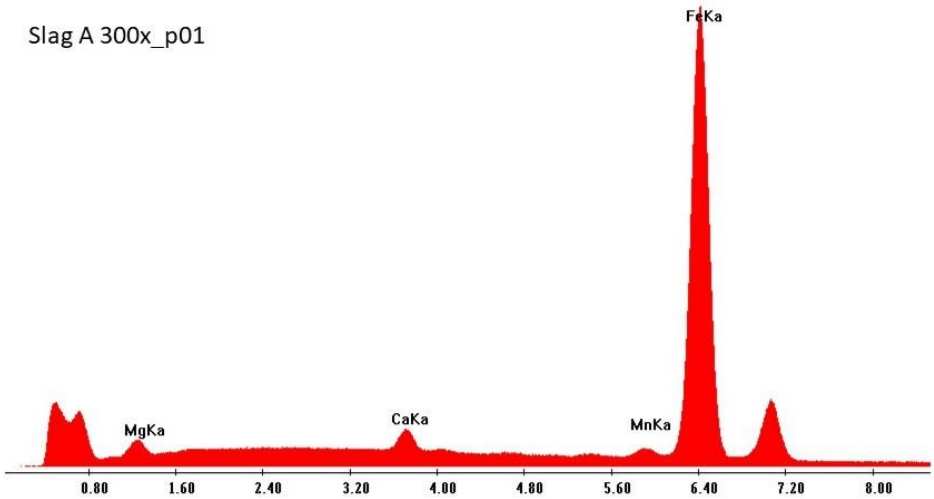

Figure 6.2B. Slag A, BSE 300x. EDS spectrum of point 01: residual iron particles.

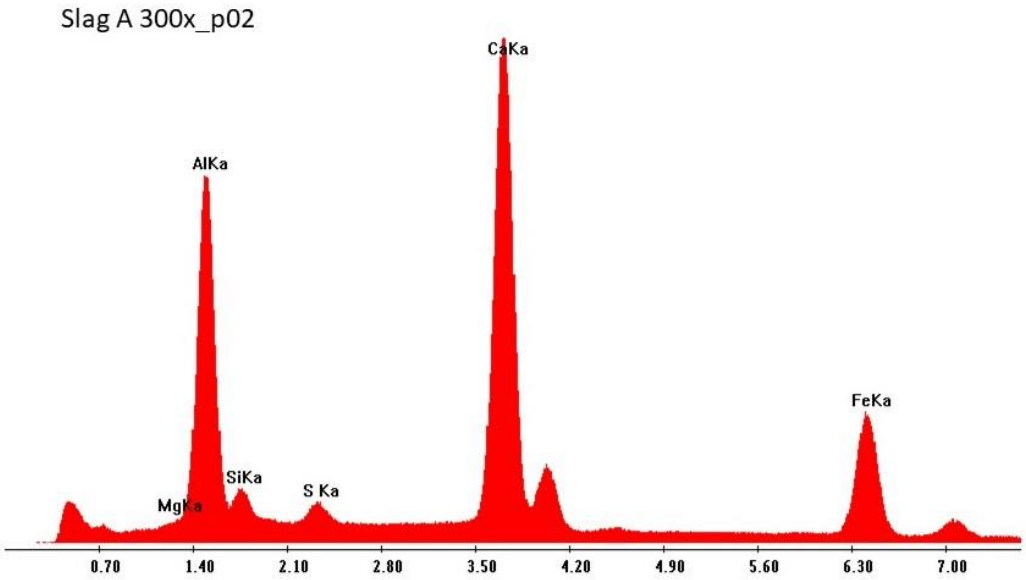

Figure 6.3B. Slag A, BSE 300x. EDS spectrum of point 02: in grains like this one, with spongy surface, a sulphur presence has been detected as we can see from the figure.

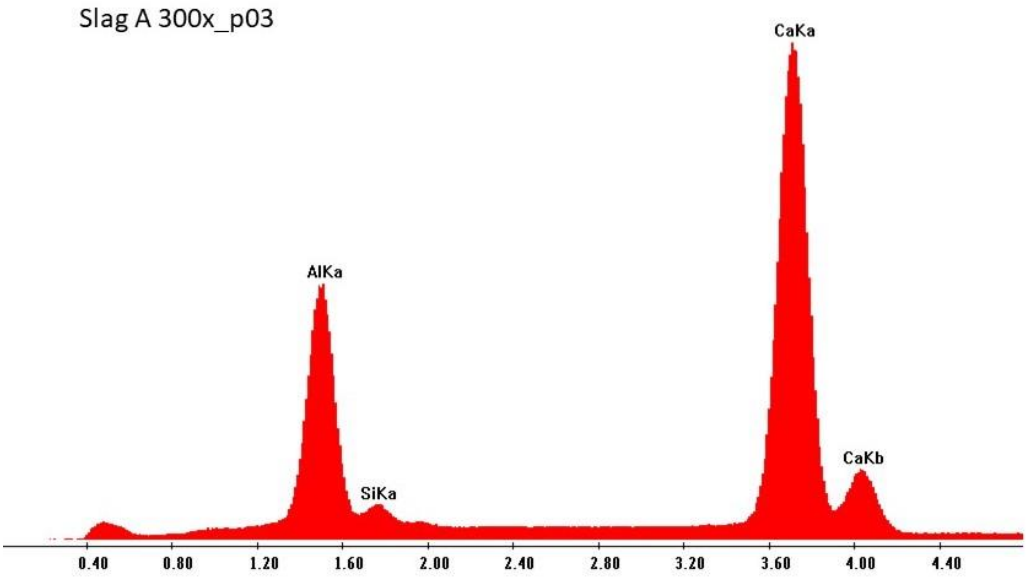

Figure 6.4B. Slag A, BSE 300x. EDS spectrum of point 03: presence of gehlenite.

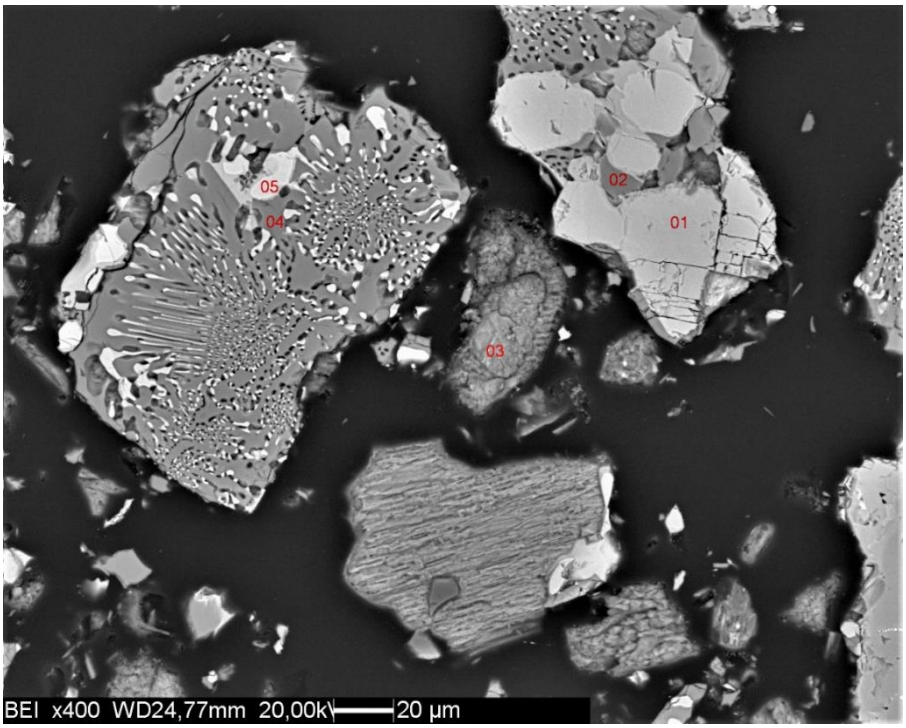

Figure 6.5B, Slag B, BSE 400x

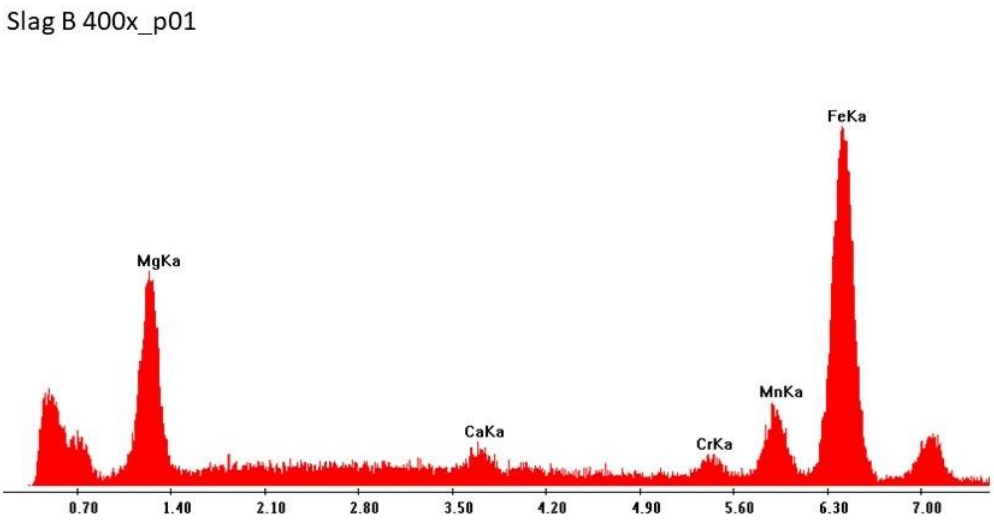

Figure. 6.6B. Slag B, BSE 400x. EDS spectrum of point 01: presence of spinels.

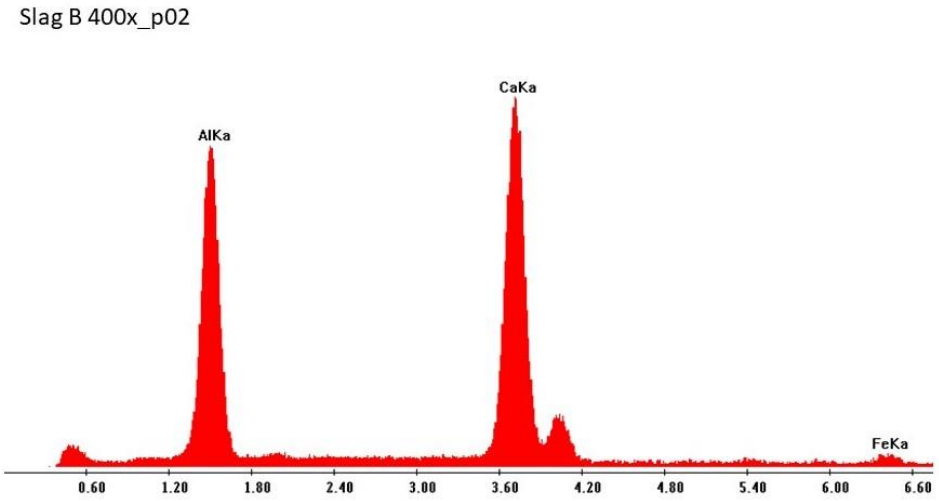

Figure *6.7B. Slag B, BSE 400x. EDS spectrum of point 02: presence of* mayenite.

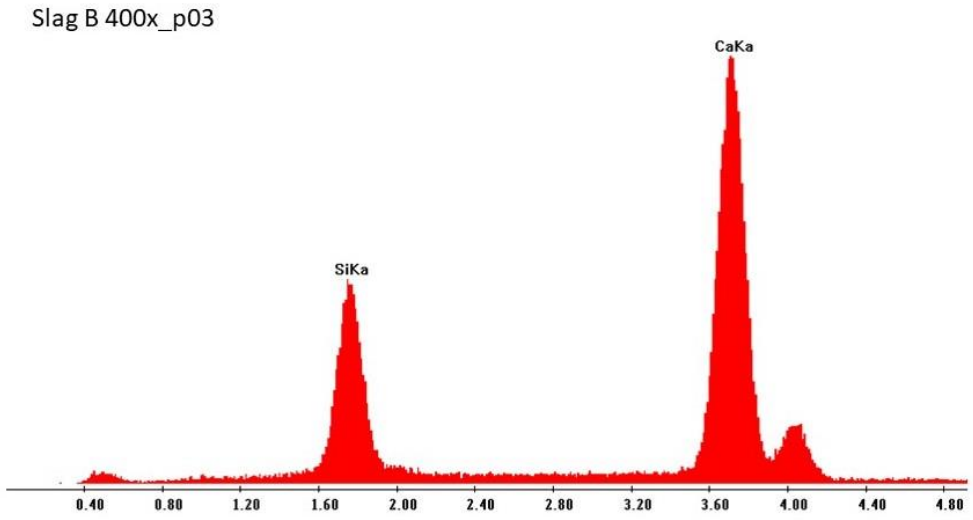

Figure *6.8B. Slag B, BSE 400x. EDS spectrum of point 03: presence of calcium-olivine.*

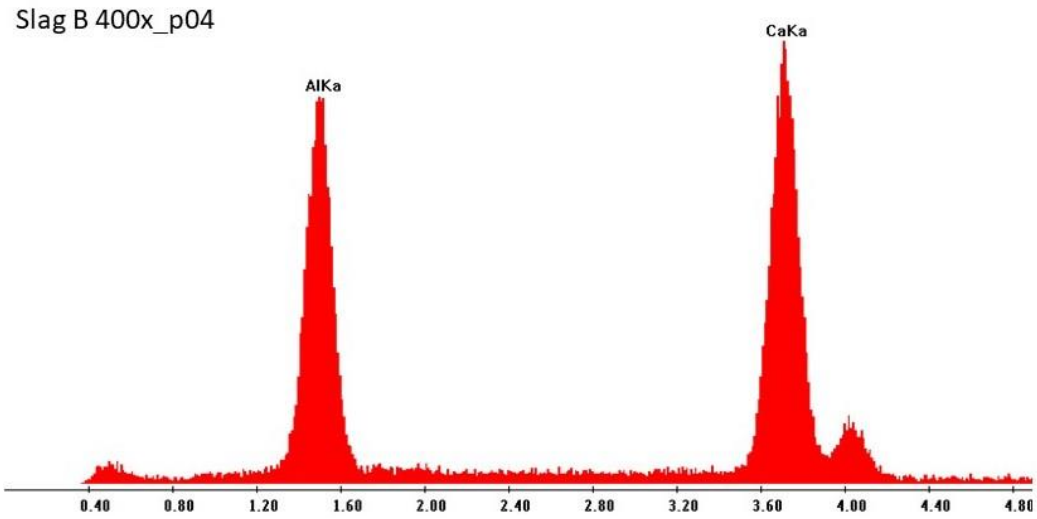

Figure 6.9B. Slag B, BSE 400x. EDS spectrum of point 04: presence of mayenite.

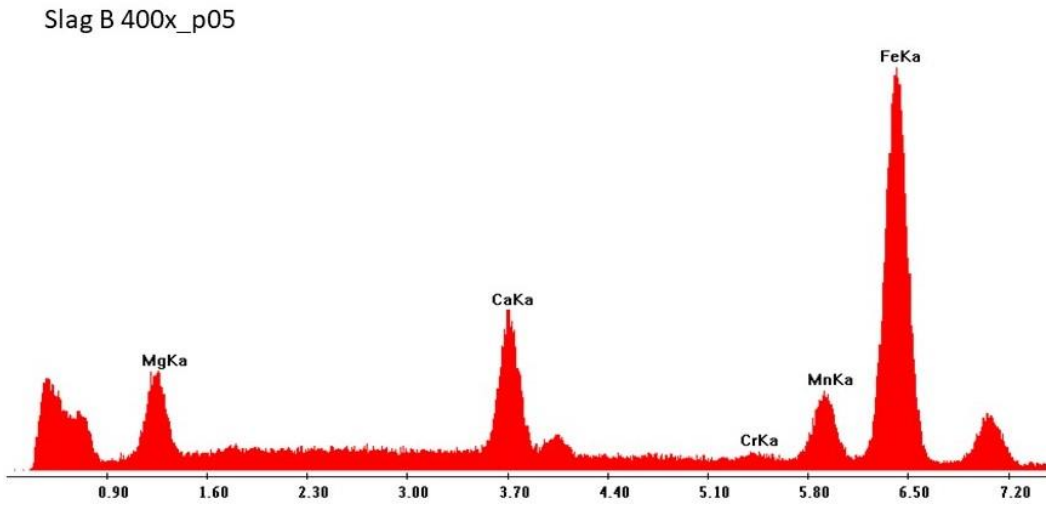

Figure 6.10B. Slag B, BSE 400x. EDS spectrum of point 05: presence of spinels.

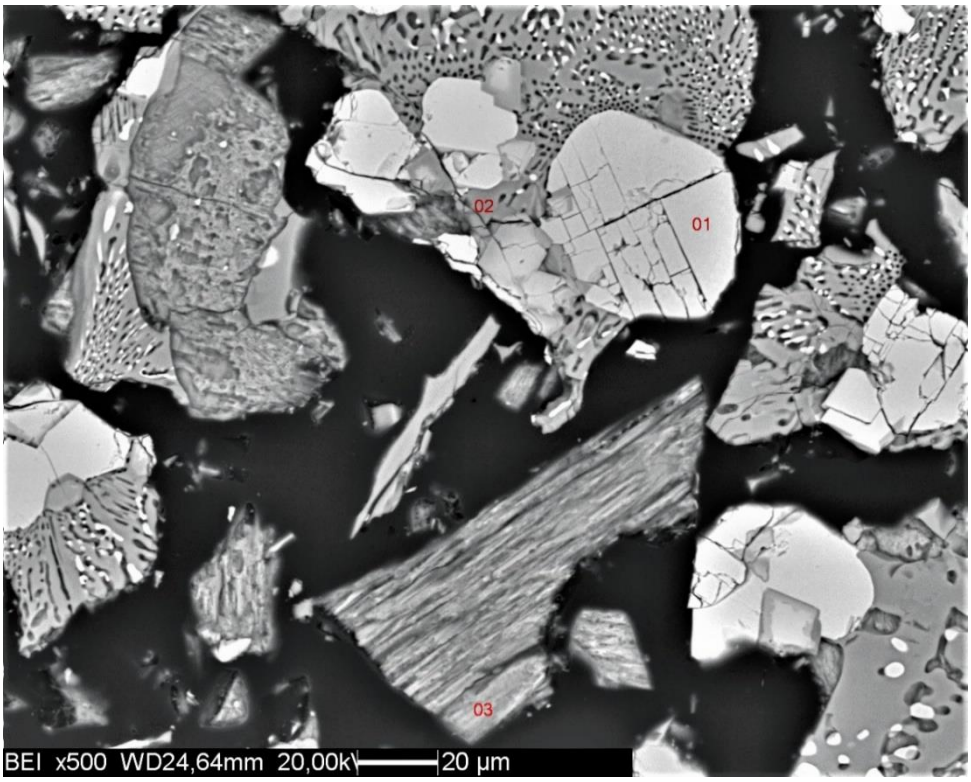

Figure 6.11B. Slag B, BSE 500x

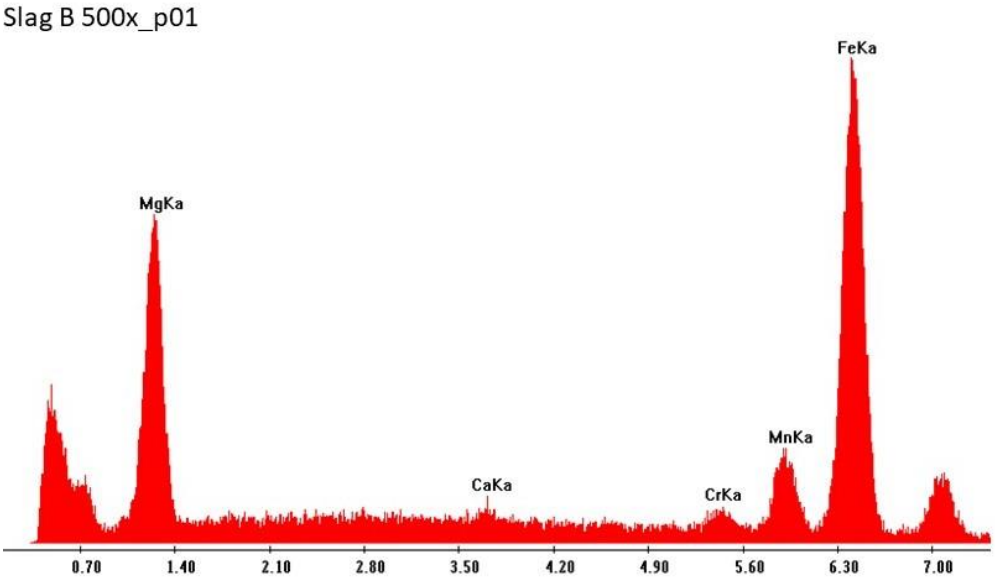

Figure 6.12B. Slag B, BSE 500x. EDS spectrum of point 01: presence of spinels.

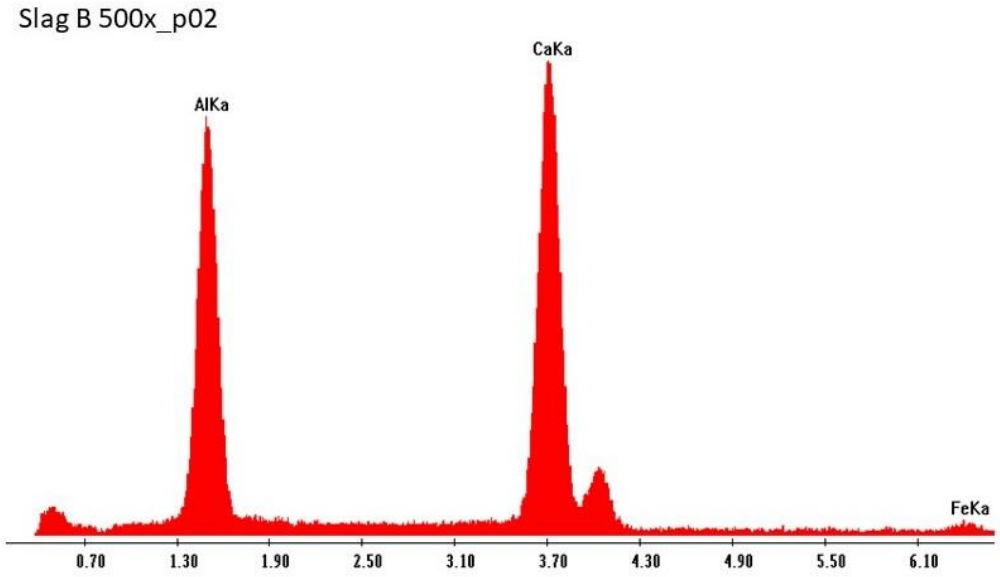

Figure *6.13B. Slag B, BSE 500x. EDS spectrum of point 02: presence of mayenite.*

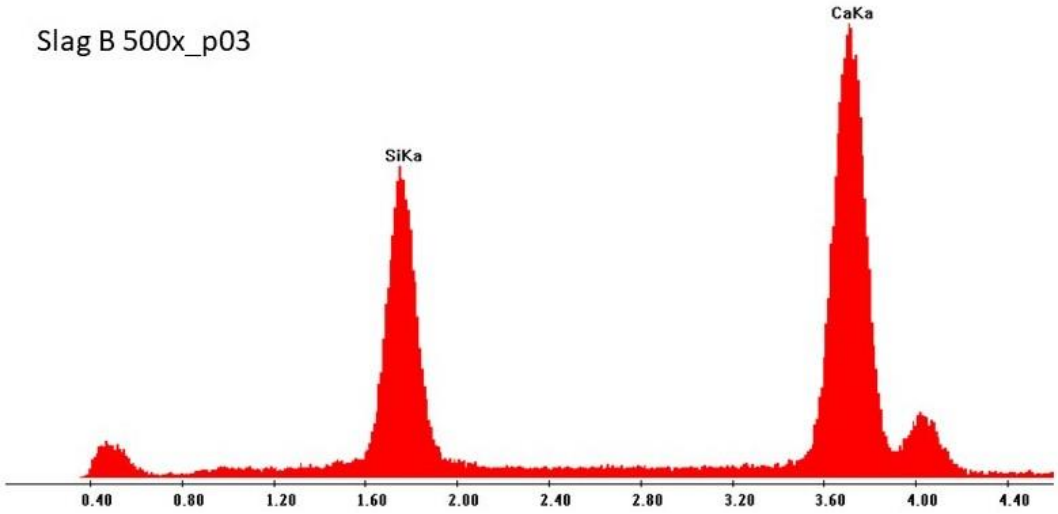

Figure *6.14B. Slag B, BSE 500x. EDS spectrum of point 03: presence of calcium-olivine.*

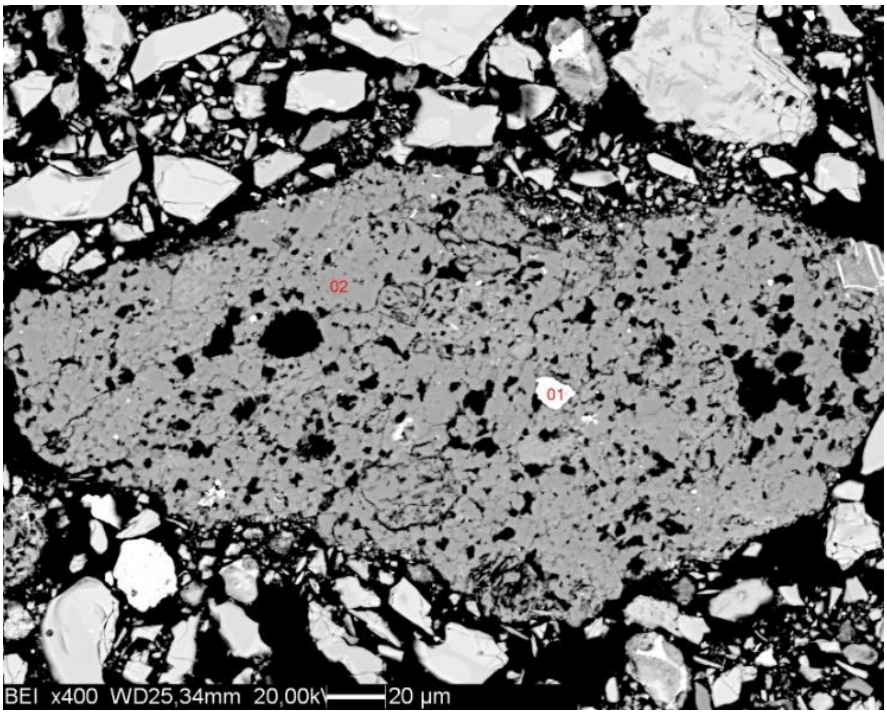

Figure 6.15B. Slag C, BSE 400x

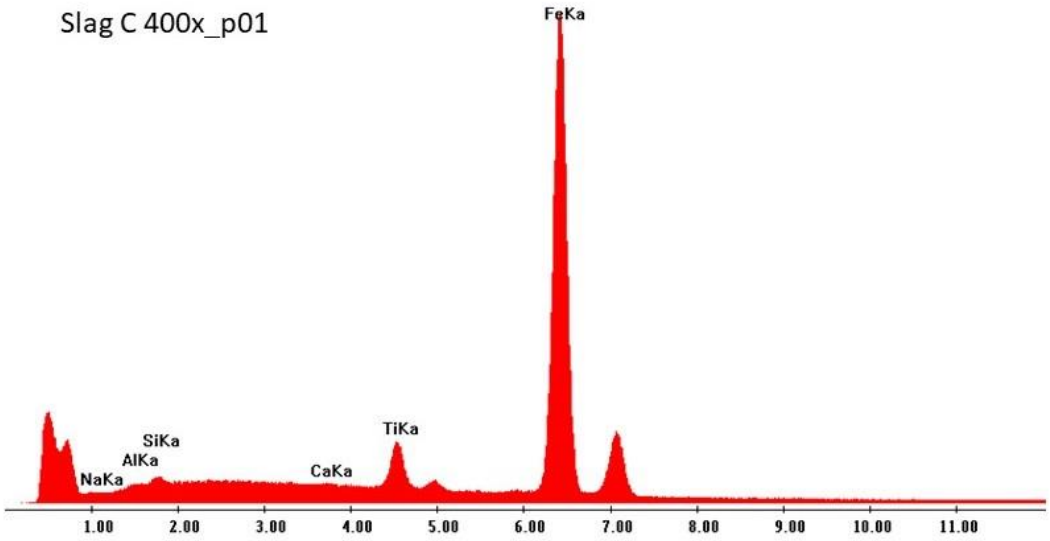

Figure 6.16B. Slag C, BSE 400x. EDS spectrum of point 01: presence of brownmillerite.

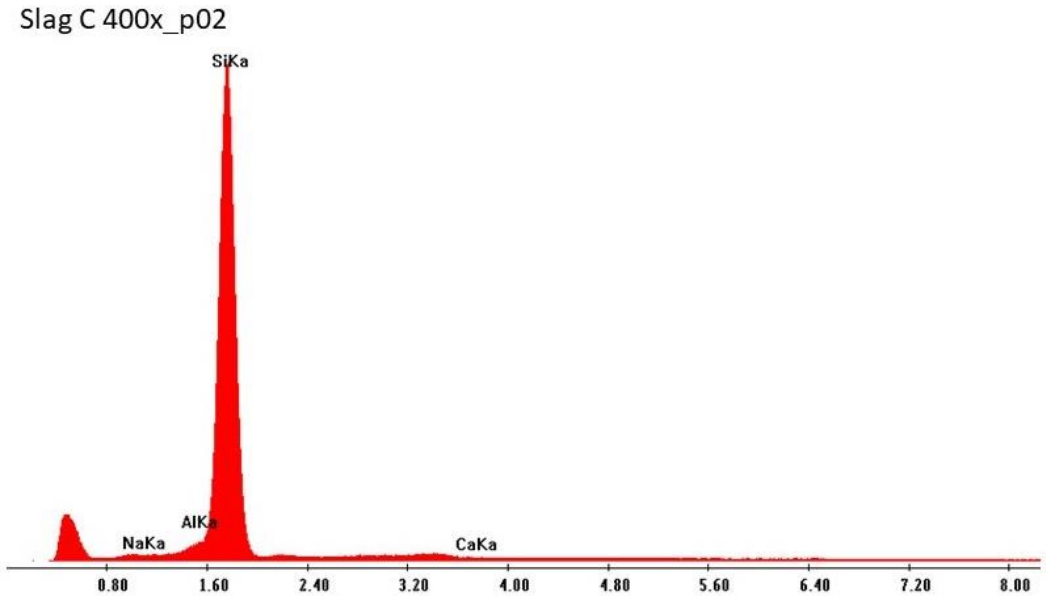

Figure 6.17B. Slag C, BSE 400x. EDS spectrum of point 02: presence of quartz.

References

Artioli, G. (2018) 'Crystal-chemistry and properties of industrial materials, Materiale Didattico A.A. 2018'.

Ashby, M. (2009) Materials and the Environment_ Eco-informed Material Choice.

Barcelo, L. et al. (2008) 'Cement and Carbon Emissions', (2008), pp. 1–15.

CICERO-Centre for International Climate and Environmental Research (2014) 'Global warming: Dwindling chances to stay below 2 degrees Celsius warming', ScienceDaily.

Dalconi, M. C. (2017) 'Applicazioni Minero-Petrografiche ai Minerali Industriali, Materiale Didattico A.A. 2017/2018'.

Van Deventer, J. S. J. et al. (2012) 'Technical and commercial progress in the adoption of geopolymer cement', Minerals Engineering. Elsevier Ltd, 29, pp. 89–104.

EN-196 Methods of testing and Cement (2005) 'Methods of testing cement'.

Euroslag (2018) www.euroslag.com. Available at: http://www.euroslag.com/.

De Jesus, A. et al. (2018) 'Eco-Innovation in the transition to a circular economy: An analytical literature review'.

Mangolini, B. (2018) Studio della fluidità di cementi ad alto contenuto in ceneri e loppe mediante disegno sperimentale. Università degli Studi del Piemonte Orientale.

Mazzoli, C. (2017) 'Applied Petrography, Materiale Didattico A.A. 2017/2018'.

Ramanathan, V. and Xu, Y. (2010) 'The Copenhagen Accord for limiting global warming: Criteria, constraints, and available avenues', PNAS, 107(18), pp. 8055–8062.

Scrivener, K., Snellings, R. and Lothenbach, B. (2016) A Practical Guide to Microstructural Analysis of Cementitious Materials.

Shi, C. (2004) 'Steel Slag — Its Production , Processing , Characteristics , and Cementitious Properties', Journal of Materials in Civil Engineering, 16(June), pp. 230–236.

Snellings, R., Mertens, G. and Elsen, J. (2012) 'Supplementary Cementitious Materials', Mineralogy & Geochemistry, 74(December 2013), pp. 211–278.

Acknowledgements/Ringraziamenti

Un’infinità di grazie alle persone che mi sono state vicino in questi anni.

Ai miei genitori: mamma Nadia e papà Renzo, per avermi sempre sostenuta e supportata (in ogni modo) in questi anni e tralasciato il mio essere superdisordinata.

A Gisella che, anche se è sempre in giro per il mondo senza di me, in qualche modo riesce a sopportarmi (ti sei meritata una marea di treatos).

Alle mie amiche di sempre Sara, Liv, Angelica, Marianna con cui ho condiviso le mie passioni, una marea di concerti, trasferte, notti passate chissàddove, viaggi infiniti, serate moleste al Vidia, gli sbronzi College Party a Bologna…non riuscirei mai ad elencare tutti i momenti trascorsi assieme (un grazie anche a Federico che ormai è nel team). Ad Anna (zamp), Nessi, Anna (gambera) e ai miei amici di concerti in giro per l’Italia, sempre pronti a fare del party.

A Mazza per essere un cuore per i disagi che abbiamo con le persone, per le date dei concerti spifferati, per i diti medi mandati con perseveranza.

A Matteo per avermi insegnato che “la vita è come la sedia del Madrid: ti ci siedi e ti ci incastri” e per avermi scritto un libro che mi insegnerà sicuramente ad evitare ancora casi umani.

A Linda, che non si sa mai dove sia, sicuramente dispersa da qualche parte in giro per il mondo, ad Alice, per essere una merda, ma con il cuore, ad Alessia e ai nostri perenni disagi con la vita e a Medi, perché tutte le strade portano a Fontanelle, l’importante è non arrivarci mai.

A tutti i miei Geoamici, che con me hanno condiviso ansie pre-esame, campi disperati, feste nebbiose, aperitivi al Civico, serate disagio sfociate in ubriachezza molesta, intense giornate di studio e sclero, partite di pallavolo alla Kioene, Geocene finite sempre non bene, vacanze, capodanni sobri e gite in montagna.

Alla mia “Famiglia Degradata” Silvia, Anna, Sofia, Leonardo, Simone (chiave grande), a Lorenzo per accettare sempre le mie malsane proposte di sobri giretti al lago dell’ultimo minuto e ai restanti amici di “Mondobueo”, Riccardo e Caterina.

Ai miei “vecchi” compagni con cui ora anche io condividerò il disagio di essere laureata e disoccupata, ma ricorderò per sempre il viaggio alle Eolie come una delle esperienze più mistiche della mia vita: Ilaria (bombe), Lucrezia, Gaia, Agnese, Pietro, Marco, Samuele, Carlo, Leonardo, Caterina, Luca, Matteo, Simone, Federico, Nicola, Edoardo.

Ai miei “nuovi” compagni con cui ho condiviso i restanti campi-disagio, partite con il TeamOlesto e Penicotteri e tutto il viaggio della magistrale: Andrea (simia), Matteo (quello terrone), Fillo, Ilaria, Marco, Antonino, Alessio, Luca, Andrea, Luca (pres), Censo, Gianni, Pette e tutti i miei Georapp preferiti.

A Isabella, Alessandro, Lorenzo (moz), Valeria, Luisa e tutte le persone conosciute nel corso di questi anni universitari, che in qualche modo hanno lasciato un segno.

Ai miei (ormai ex) colleghi di Osteria: Lorenzo, Jerry, Marta ed Emanuela (bubuki), per le serate a lavoro sfociate in disagio, alle creme al mascarpone e cantucci, ai post-serata al Fish, ai limoncelli rubati e alle chiacchiere estive quando eravamo i padroni di via Altinate.

Un grazie particolare va a tutte le persone che hanno contribuito alla realizzazione di questo lavoro: al mio relatore Prof. Gilberto Artioli, ai miei correlatori Dott. Maurizio Bellotto e Dott.ssa Maria Chiara Dalconi, al Dott. Enrico Garbin e a tutto il team di ricerca CIRCe. Un ulteriore ringraziamento a Federico Zorzi, Leonardo Tauro, Marco Favero e a tutte le persone che mi hanno aiutata con le analisi in laboratorio.

Veronica